Investigations on the influence of dry lubes in warm forming of high and ultra-high strength steels

Marco Dal Mutto

Master Thesis 2012/2013

Matriculation number: 1020344

Supervisor: Ing. Andrea Ghiotti

Contents

List of used variables, symbols and abbreviations

Symbol	**Unit**	**Explanation**
D_0	mm	Initial external blank diameter
D	mm	Actual external blank diameter
d_d	mm	Die diameter
d_p	mm	Punch diameter
r_d	mm	Die radius
r_p	mm	Punch radius
u_d	mm	Die clearance
t_0	mm	Sheet thickness
β_0	-	Initial drawing ratio
β	-	Actual drawing ratio
ε	-	Engineering strain
σ	MPa	Engineering stress
φ	-	True strain
k_f	MPa	Flow stress
μ		Coefficient of friction
w	mm	Width of the tensile test specimen
l	mm	Length of the tensile test specimen
v	mm/s	Velocity
BHF	N	Blank holder force

1 Introduction

In the automotive industry, the weight of a component plays an important role in emissions reduction and fuel consumption. Focusing on this target, high and ultra-high strength steels assume a very important function. Indeed they allow a reduction of the weight of the vehicle, without influencing safety and crashworthiness qualities. These materials, on one hand are characterized by high performances; on the other hand they have some manufacturing limits that can be reduced by a strategic use of temperature.

Forming limits of ultra-high strength steel can indeed be increased significantly by warm forming operations. Beside the positive effect of reduced forming forces, and the consequent problem of modify the machines to make them temperature supported, also an increment of friction coefficient can be observed for elevated temperatures. These higher friction coefficients for the contact between blank and tool components reduce blank drawing formability. For elevated temperatures, the exploitation of oils in order to decrease friction is not appropriate. Taking this into account, dry lubes like graphite or boron nitride, which are temperature-stable at these temperatures, have to be characterized as lubricants.

2 State of the art

2.1 Deep drawing

Deep drawing is a manufacturing process in which a metal sheet is forced into a die with cylindrical or rectangular shape. A cylindrical sheet of metal with diameter D_0 and thickness s_0 is placed over the die with radius R_d. The die is held by a blank holder by means of a vertical force. The blank holder is needed also to prevent wrinkles that can occur during the process. Winkles are generated by material flowing into a three-dimensional shape characterized by huge shape changes.

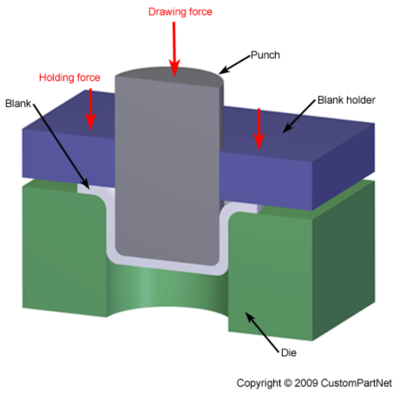

Figure 1 deep drawing component

The cylindrical final shape is due to the vertical movement of a punch with diameter D_p and radius R_p, which forces the piece inside the die. All the forces and the kinematics are generated by means of a mechanical or hydraulic press.

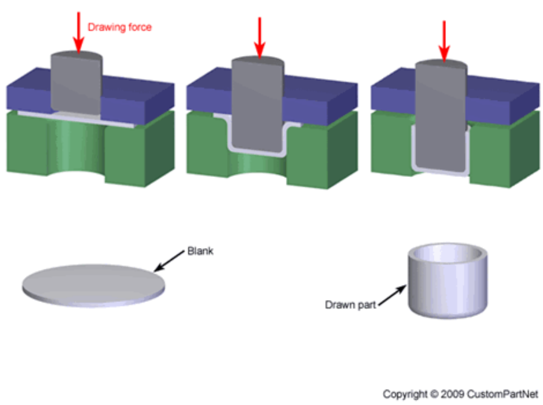

Figure 2 cup formation

This process is suitable for the production of final workpieces that can be assembled without further operations. The development of specific methods has paralleled general technological development, especially in the automotive and aircraft industries. Deep drawing is characterized by a rapid press cycle time and complex axisymmetric pieces. Also non-symmetrical geometries can be realized. This process is the most widely used sheet metal working process. It can produce both small pieces for the electronic industry and pieces with dimensions of several meters.

The independent variables of the deep drawing process are:

- Characteristics of the metal sheet
- Drawing ratio (ratio between piece diameter and punch diameter)
- Thickness of the metal sheet
- Clearance between punch and die
- Blank holder force
- Friction in the interface between punch, die and metal sheet
- Punch velocity

During the process the component is subjected to different state of stress.

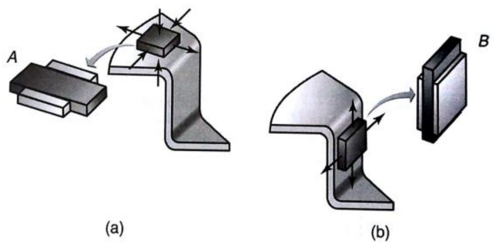

Figure 3 state of stress (Serope Kalpakjian, 2008)

In element A, the radial tensile state of stress is due to the fact that the metal sheet is forced into the die and the compression state of stress in normal direction of the element is due to the pressure of the blank holder. The radial tensile stress leads to a compression state of stress in the circumferential direction. As a consequence of the stress state, the element A contracts in the circumferential direction and stretch in the radial direction. The compression state of stress in the circumferential direction that takes place in the flange area tends to cause the formation of wrinkles. To avoid this problem, a blank holder is needed.

In element B, the walls of the cup are subjected to tensile stress. The punch transmits the drawing force to the material in the flange area through the wall of the component. The tensile stress in the circumferential direction of the element B is the consequence of the reduction of the cup diameter due to the tensile stress that tends the material to adhere to the wall of the punch.

2.1.1 Deep drawing at elevated temperatures

Metal sheets with high strength can be formed at elevated temperature in order to increase ductility and reduce the needed force of deformation and the spring back. As a consequence of these higher characteristics the quality of the products can be increased.

Warm processes are those processes in which the material is formed under the recrystallization temperature. Improvements of forming property are realized without structural changes. An advantage obtained by applying this kind of process is that no cooling curves have to be used because the head treatments are not conditioned.

Before forming, the specimen is heated and afterward it is formed by a punch and a heated die. The punch can be occasionally cooled so the drawn component is as strong as possible in the transition region from the bottom to the wall of the cup and it can transmit high drawing loads.

Forming at elevated temperature is a very costly process and the metal sheet has to be coated to prevent oxidation or it has to be conducted in inert atmosphere. In addition, for temperature above 400 °C there is an increase of friction. Therefore it has to be evaluated if the increment of temperature is really convenient and it has to be carried out an accurate analysis in order to determine which lubricant-temperature combination is optimal.

2.2 *Friction in forming process*

Friction is the force resisting to the relative motion of material element sliding each other under a normal force. Any metal forming process is subject to friction, because of the relative motion, and the forces between tools, dies and pieces. Friction entails energy dissipation and consequently heat generation and increment of forces.

In deep drawing process, the flange is the region subjected to the higher friction. Lubricant is very important because it influences:

- Thickness and possible failure of the wide wall in the drawn cup,
- The draw in length on the flange.

The contribution of friction in the total force of deformation is often less than 5% but with high temperature its influence is higher. It is very important to evaluate the value of such contributions because otherwise it would be impossible to accurately compute the amounts of forces and energy needed for the process.

Several theories for friction phenomena exist and they are valid if they can explain the friction effects between the surfaces as the operating conditions change, e.g. applied loads, sliding speed, temperature etc.. An elementary model for the friction explanation is provided by Coulomb´s model, according to which the friction is due to the mechanical interaction between the asperities of the surface in contact, which cause a resistance in the relative sliding of the surfaces.

A more advance friction model that has a good agreement with the experiments is based on adhesion phenomena. According to this model, the contact area between metal surfaces is just a portion of the nominal contact area, so the static load at the interface is sustained only by the contact asperities. The total contact area is named real contact area A_r. For low normal load and with a vast real contact area the stress on the asperities is low and so they are in the elastic field. As the normal load increases also the stress on the asperities increases and they can plastically deformed. In this case the contact area grows and new asperities get in touch. Strong contact of asperities generates adhesive bonds that involve atomic interactions, mutual solubility and diffusion.

2.2.1 Friction coefficient

The relative motion of body elements sliding each other under a normal force N, is possible only by means of a tangential force F. The adhesive theory affirms that F is the shear force needed to break the junction at it is called friction force.

The friction coefficient at the interface is defined as the adimensional ratio between the shear stress τ and the normal stress σ.

$$\mu = \frac{F}{N} = \frac{\tau \cdot A_r}{\sigma \cdot A_r} = \frac{\tau}{\sigma} \qquad [\ 1\ ]$$

in which A_r is the contact area between the two surfaces.

The friction coefficient μ is usually used as a main indicator, it depends on:

- the material
- the contact surface
- the lubricant
- the normal pressure on the contact surface.

Practical values of the friction coefficient vary from 0,02 to values greater than 100 (Serope Kalpakjian, 2008). This high range is due to the number of factors that influence the friction.

2.2.2 Friction factor

When two cleaned surfaces are forced against each other, a welding effect may be induced by cold pressure, if the pressure itself is enough high. If the normal force N is further increased, the friction force F remains constant. As a consequence the friction factor decreases. This condition explains why a more realistic way to represent the friction condition at the interphase is used. A valid approach is to define a friction factor m:

$$m = \frac{\tau_i}{k} \qquad [\ 2\ ]$$

In which τ_i is the shear strength at the interface and k is the shear yield stress.

The friction factor can vary between $m = 0$ without friction and $m = 1$ with complete adhesion.

2.3 Plasticity theory equations of Siebel

The required drawing loads and their variations along the punch stroke can be determined in two ways, either from theoretical equations based on plasticity theory, or by using empirical equations. In this investigation the Siebel´s analytical equation is used and it is calculated with the following assumptions:

- Constant thickness of sheet during the process
- Linear hardening
- Tresca’s yield criterion
- Rope friction force equation for the calculation of the friction force at the radius of the die
- Ideal plastic behavior of the material in the bending and back-bending calculation
- Isothermal process.

2.3.1 Ideal force of deformation

2.3.1.1 Shape changes in the flange

For the computation of the ideal force of deformation in the flange area, shape changes in this area and in the correspondent strain have to be evaluated. In Figure 4 there are two different parts of the flange, in which the thickness s_0 is assumed to be constant.

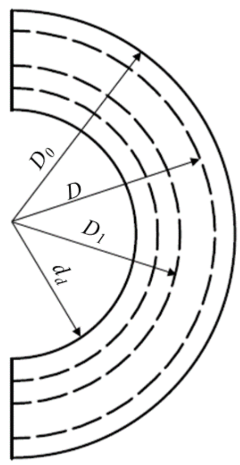

Figure 4 shape changes in flange area

The inner and the outer areas are considered equal and so it is possible to obtain the following relationships:

$$\frac{\pi}{4}\left(D_0^2 - D^2\right) = \frac{\pi}{4}\left(D_1^2 - d_p^2\right) \qquad [\ 3\ ]$$

from which follows that

$$D_1^2 = D_0^2 - D^2 + d_p^2 \qquad [\ 4\ ]$$

$$\frac{D_1^2}{d_p^2} = \frac{D_0^2}{d_p^2} - \frac{D^2}{d_p^2} + 1 \rightarrow \frac{D_1^2}{d_p^2} = \left(\frac{D_0}{d_p}\right)^2 - \left(\frac{D}{d_p}\right)^2 - 1 \qquad [\ 5\ ]$$

In which

$$\beta_0 = \frac{D_0}{d_p}\ and\ \beta = \frac{D}{d_p} \qquad [\ 6\ ]$$

By combining the previous equations, it is possible to obtain:

$$D_1^2 = \beta_0^2 \cdot d_p^2 - \beta^2 \cdot d_p^2 + d_p^2 \qquad [\ 7\ ]$$

$$\frac{D_1^2}{d_p^2} = \beta_0^2 - \beta^2 + 1 \qquad [\ 8\ ]$$

Finally for the inner and outer radius the true stain results:

$$\varphi_1 = ln\frac{D_1}{d_p} = ln\sqrt{\beta_0^2 - \beta^2 + 1} \qquad [\ 9\ ]$$

$$\varphi_2 = ln\frac{D_0}{D} = ln\frac{\beta_0}{\beta} \qquad [\ 10\ ]$$

(Eckart Doege, 2010)

2.3.1.2 Evaluation of pure plastic stress of deformation

The radial stress σ_r in the flange can be calculated from equilibrium equation:

$$\sigma_r \cdot r \cdot d\alpha \cdot t_0 - (\sigma_r + d\sigma_r) \cdot (r + dr) \cdot d\alpha \cdot t_0 + 2 \cdot \sigma_t \cdot t_0 \cdot \frac{d\alpha}{2} \cdot dr = 0 \quad [\ 11\ ]$$

From which follows that:

$$-d\sigma_r \cdot r - \sigma_r \cdot dr - d\sigma_r \cdot dr + \sigma_t \cdot dr = 0 \quad [\ 12\ ]$$

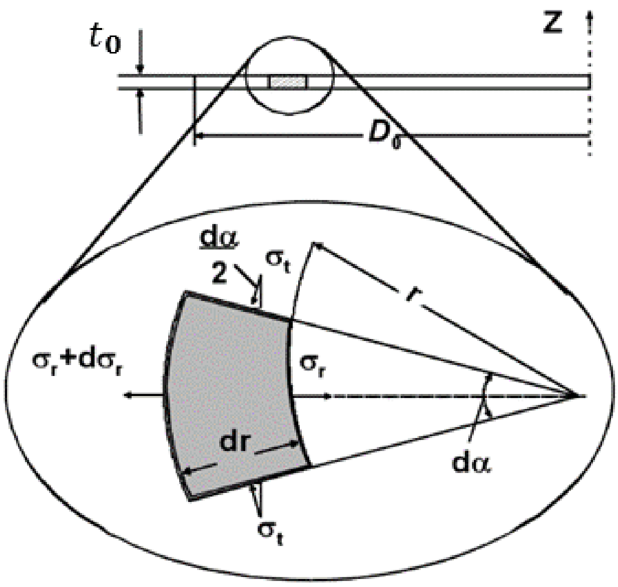

Figure 5 2.3.1.2 Evaluation of pure plastic stress of deformation (Eckart Doege, 2010)

Neglecting the upper order term, it is possible to suppose:

$$d\sigma_r \cdot dr = 0 \quad [\ 13\ ]$$

And finally it is possible to obtain

$$d\sigma_r = -(\sigma_r - \sigma_t) \cdot \frac{dr}{r} \quad [\ 14\ ]$$

The radial stress using the Tresca's yield criterion $k_f = \sigma_{max} - \sigma_{min}$ results in:

$$\sigma_r(r) = -\int_{r=R}^{r_0} k_f(r) \cdot \frac{dr}{r} = -k_{fm} ln\left(\frac{r_p}{R}\right) = k_{fm} \cdot ln\left(\frac{D}{d_p}\right) \qquad [\ 15\ ]$$

in which K_{fmI} is the average stress in the deformation between outer and inner radius of the flange. It is a function of the punch stroke and it is calculated as follows:

$$k_{fmI} = \frac{1}{\varphi_2 - \varphi_1} \int_{\varphi_1}^{\varphi_2} k_f(\varphi) d\varphi \qquad [\ 16\ ]$$

The tangential stress can be calculated as:

$$k_{fmI} = \sigma_r - \sigma_t \rightarrow \sigma_t = \sigma_r - k_{fm} \qquad [\ 17\ ]$$

(Eckart Doege, 2010)

2.3.1.3 Ideal force of deformation

The Tresca´s yield criterion gives flow conditions that are lower, 10% on the average, than the criterion of Von Mises.

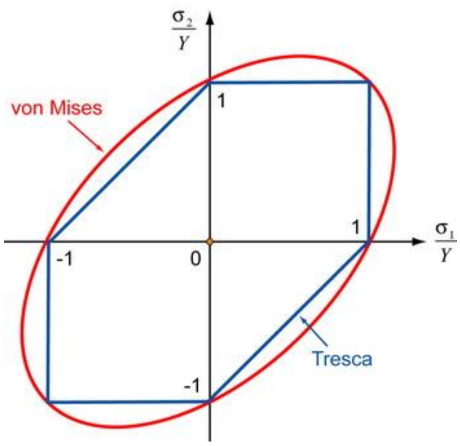

Figure 6 Von Mises and Tresca yield criterions

If a correction factor 1,1 is used, the radial stress becomes:

$$\sigma_{r,id} = 1{,}1 \cdot k_{fmI} \cdot \ln(\beta) \quad [\,18\,]$$

Multiplying the stress by the transversal area of the wall (portion of the blank being drawn into the cavity) it is possible to calculate the punch force needed for the deformation on the flange:

$$F_{id} = \sigma_{r,id} \cdot A = \pi \cdot (d_p + \frac{t_0}{2}) \cdot s_0 \cdot 1{,}1 \cdot k_{fmI} \cdot \ln(\frac{D}{d_p}) \quad [\,19\,]$$

(Eckart Doege, 2010)

2.3.2 Bending force

The bending moment is obtained from the equation of Navier for the calculation of the stress generated from a bending moment

$$\sigma_b = \frac{M_b \cdot x}{J} \quad [\,20\,]$$

where x is the distance from the neutral line, M_b the bending moment and J the moment of inertia of the section respect to the neutral line and distance x. In case of a rectangular section with width b the bending moment becomes:

$$\sigma = \frac{M_b \cdot \frac{t_0}{2}}{\frac{t_0^3 \cdot b}{12}} \rightarrow M_b = \frac{\sigma \cdot {t_0}^2 \cdot b}{6} \quad [\,21\,]$$

In case of complete plastic deformation the bending moment generates a stress distribution that is constant with value $+k_f$ above the neutral line and with value $-k_f$ below the neutral line

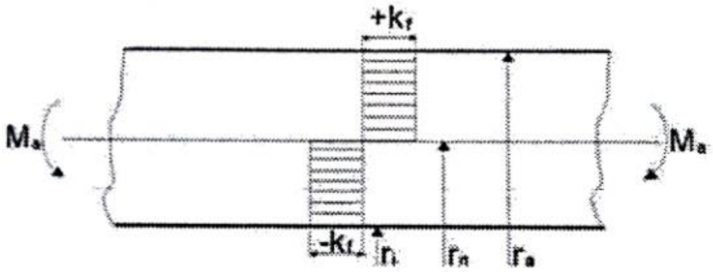

Figure 7 stress in bending (Z.Hu, 2003)

In this condition the bending moment has to be multiplied by a coefficient that is 1,5 for rectangular section. The bending moment therefore becomes:

$$M_b = \frac{k_{fmII} \cdot b \cdot t_0^2}{4} \quad [\ 22\ ]$$

where k_{fmII} is the average value of strain calculated before and after bending.

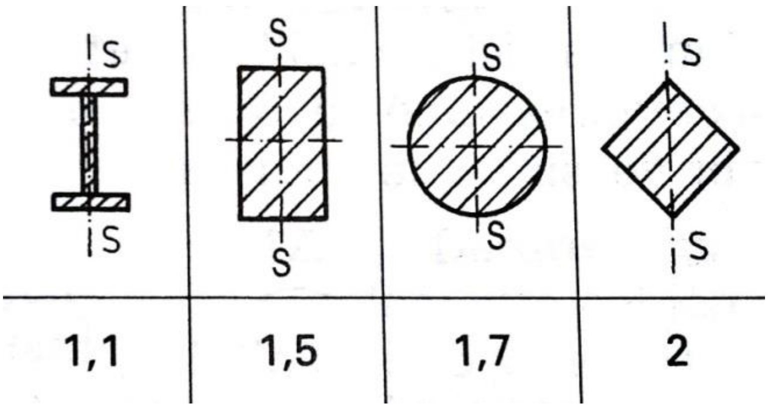

Figure 8 coefficient for plastic stress calculation (Andreini, 2002)

The bending stress is calculated dividing the bending moment for his arm and the transversal area of the considered element.

$$F_b = \frac{M_b}{r_d + \frac{t_0}{2}} = \frac{k_{fmII} \cdot b \cdot t_0^2}{4 \cdot \left(r_d + \frac{t_0}{2}\right)} \cong \frac{k_{fmII} \cdot b \cdot t_0^2}{4 \cdot r_d} \quad [\ 23\ ]$$

$$\sigma_b = \frac{k_{fmII} \cdot t_0}{4 \cdot (r_d)} \quad [\ 24\ ]$$

Multiplying the bending stress for the transversal area of the wall, the force needed to bend the blank is computed as:

$$F_b = \sigma_b \cdot A = \pi \cdot (d_p + \frac{t_0}{2}) \cdot s_0 \cdot \frac{k_{fmII} \cdot t_0}{4 \cdot (r_d)} \quad [\ 25\ ]$$

(Eckart Doege, 2010)

2.3.3 Back bending force

After the bending the sheet is back bended. As a consequence of a plastic deformation of the material, the back bending force has to be considered and it is equal to the bending force, assuming that the material does not work harden.

$$F_{bb} = \sigma_{bb} \cdot A = \pi \cdot (d_p + \frac{t_0}{2}) \cdot s_0 \cdot \frac{k_{fmII} \cdot t_0}{4 \cdot (r_d)} \qquad [\ 26\ ]$$

2.3.4 Friction force between the blank holder and the die

The friction force between the blank holder and the die is calculated from the blank holder force using the Coulomb's Law:

$$F_{ff} = 2 \cdot \mu \cdot F_{bh} \qquad [\ 27\ ]$$

Where F_{bh} is the blank holder force and F_{ff} is the related friction force.
The friction stress is obtained dividing the force for the transversal area:

$$\sigma_{ff} = \frac{F_{ff}}{\pi \cdot D \cdot t_0} = \frac{2 \cdot \mu \cdot F_{fh}}{\pi \cdot D \cdot t_0} \qquad [\ 28\ ]$$

The friction force acts in the opposite direction of the movement of the flange and so it has to be considered the external transversal area for the calculation of the stress.
Multiplying the friction stress for the transversal area of the wall:

$$F_{ff} = \sigma_{ff} \cdot A = \pi \cdot (d_p + \frac{t_0}{2}) \cdot t_0 \cdot \frac{2 \cdot \mu \cdot F_{fh}}{\pi \cdot D \cdot t_0} \qquad [\ 29\ ]$$

(Eckart Doege, 2010)

2.3.5 Friction's effect at the radius of the die

The effect of friction at the radius of the die generates a surplus of needed force of the punch and it is calculated using the rope friction force.

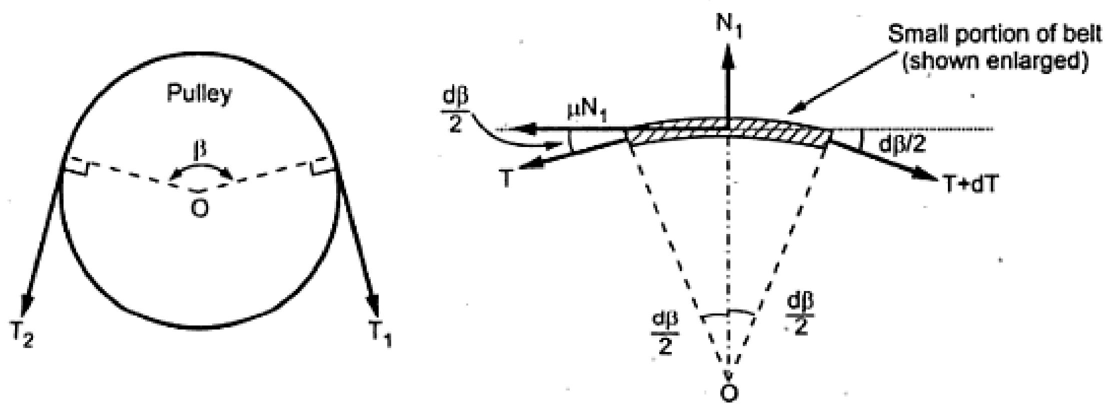

Figure 9 rope friction calculation (Nisture, 2006)

From the radial equilibrium equation of an infinitesimally portion of the rope:

$$N - T \cdot sin\left(\frac{d\alpha}{2}\right) - (T + dT) \cdot sin\left(\frac{d\alpha}{2}\right) = 0 \qquad [\ 30\ ]$$

Considering the infinitesimally portion investigated it is possible to approximate as follows

$$sin\left(\frac{d\alpha}{2}\right) \approx \frac{d\alpha}{2} \qquad [\ 31\ ]$$

So

$$N = T\left(\frac{d\alpha}{2}\right) + (T + dT)\left(\frac{d\alpha}{2}\right) = T \cdot d\alpha + dT \cdot \frac{d\alpha}{2} \qquad [\ 32\ ]$$

which by approximation becomes

$$N = T \cdot d\alpha \qquad [\ 33\ ]$$

From the tangential equilibrium of the same portion:

$$(T + dT) \cdot cos\left(\frac{d\alpha}{2}\right) - T \cdot cos\left(\frac{d\alpha}{2}\right) - \mu N = 0 \qquad [\ 34\ ]$$

Replacing the normal force with the value calculated before:

$$(T + dT) \cdot cos\left(\frac{d\alpha}{2}\right) - T \cdot cos\left(\frac{d\alpha}{2}\right) - \mu T \cdot d\alpha = 0 \qquad [\ 35\ ]$$

Considering the infinitesimally portion investigated it is possible to approximate as follows

$$cos\left(\frac{d\alpha}{2}\right) \approx 1 \qquad [\ 36\ ]$$

$$dT = \mu(T \cdot d\alpha) \rightarrow \frac{dT}{T} = \mu d\alpha \qquad [\ 37\ ]$$

Integrating the equations it is possible to explicit the friction force:

$$\int_{T_2}^{T_1} \frac{dT}{T} = \mu \cdot \int_0^{\alpha} d\alpha \qquad [\ 38\ ]$$

$$lnT_1 - lnT_2 = \mu \cdot \alpha \rightarrow ln\left(\frac{T_1}{T_2}\right) = \mu \cdot \alpha \qquad [\ 39\ ]$$

$$T_1 = T_2 \cdot e^{\mu\alpha} \qquad [\ 40\ ]$$

Follows

$$F = (F_{id} + F_b) \cdot e^{\mu\alpha} \qquad [\ 41\ ]$$

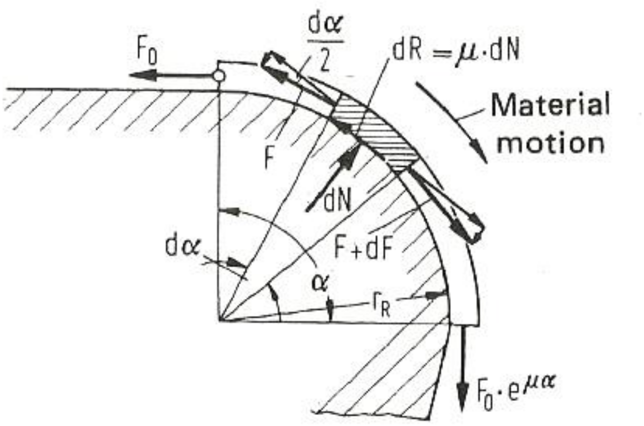

Figure 10 friction’s effect at the die radius

In this case α=π/2 so:

$$F = (F_{id} + F_b) \cdot e^{\mu\frac{\pi}{2}} \qquad [\ 42\ ]$$

(Nisture, 2006)

2.3.6 Total punch force

The total force of the punch is evaluated taking into account the following forces previously computed:

- Ideal force of deformation in the flange area,
- Bending force,
- Back banding force,
- Friction force between the black holder and the die,
- Friction’s effect at the radius of the die.

The resulting total force of the punch becomes:

$$F = \pi \cdot (d_m) \cdot t_0 \left[e^{\mu\frac{\pi}{2}} \cdot \left(1{,}1 \cdot k_{fmI} \cdot \ln\left(\frac{D}{d_m}\right) + \frac{2 \cdot \mu \cdot F_{fh}}{\pi \cdot D \cdot t_0} \right) + \frac{k_{fmII} \cdot t_0}{2 \cdot (r_d)} \right] \qquad [\ 43\ ]$$

3 Objective

The objective of this study is the evaluation of the friction coefficient of two high strength steel, CP-W800 and MS-W1200, with the utilization of different dry lubricants, graphite and boron nitride, by means of cup deep drawing test at elevated temperatures.

The investigation is conducted by means of numerical simulation for the prediction of the maximum drawing force applied to the punch in the cup deep drawing tests varying the friction coefficient in the interface between blank and the tools. The same investigation is computed also by means of the theoretical equation of Siebel for the prediction of the maximum drawing load based on the plasticity theory. The results of the two different approaches are compared and analyzed. In order to apply such an analysis, the following tests need to be carried out:

- Tensile tests at room temperature and elevated temperatures (400 °C, 500 °C, 600 °C),
- Cup deep drawing tests at room temperature and elevated temperatures (400 °C, 500 °C, 600 °C).

The tensile tests are needed for the characterization of the materials at room temperature and at high temperature. The materials indeed show a different stress-strain behavior for the different conditions and in particular as the temperature increases the strength decreases and the material can reach a higher elongation before breaking.

The cup deep drawing tests are conducted with practical stamping operations parameters focusing in particular on the punch force. It is possible indeed to evaluate the friction coefficient matching the maximum punch force resulted from the experiments with the one computed by means of the numerical simulation and the analytical equations. Once such experiments are performed, it is possible to proceed with:

- Qualitatively comparison of the behavior of the different lubricants by means of the comparison of the maximum punch force in the cup deep drawing test
- The calculation of friction coefficients by numerical simulation using a 2D axisymmetric model and the material characteristics evaluated by the tensile tests
- The comparison of the different friction coefficients in the different lubrications and

temperature conditions

- The calculation of friction coefficients by means of the analytical equation of Siebel using the flow curves of the materials evaluated by the tensile tests and the evolution of the external diameter of the flange area calculated experimentally conducting the tests at different drawing depths

Conducting the investigation with two different approaches can consent to evaluate the reflection of the different approximation of the models in the results and to have a confirmation of the goodness and validity of the results.

4 Used materials, tools and machines

4.1 High strength steels

The high and ultra-high strength steels consent the reduction on weight thanks to their developed final mechanical properties. For this reason they are extensively used in automotive industry, in particular for chassis components, like A-pillar, B-pillar, bumper, roof rail, and tunnel.

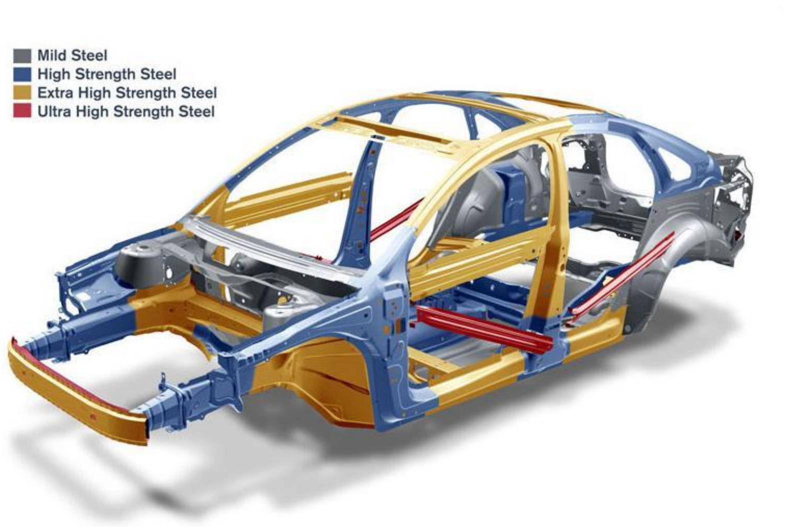

Figure 11 example of application of high strength steels

These materials show some forming capabilities and characteristics issues, such as a limited formability and a significant spring back compared with mild deep drawing steels.
As a consequence of these properties, higher force and greater dimensional deviation are needed for the manufacturing and consequently huger machine.
The strategic use of temperature can mitigate these problems reducing the needed forced and increasing the quality of the pieces.
In this study two commercial materials are analyzed: the martensitic steel MS-W1200 and a complex-phase steel CP-W800. They are both Zinc coated to prevent the oxidation and so an inert atmosphere is not needed during the processes.

4.1.1 CP-W800 complex phase steel

The CP-W800 is a high-strength hot-rolled strip steel with ultimate tensile strength of 900

MPa in the thermomechanically treated condition. Due to its chemical composition and to the special rolling process used in its manufacture this steel have an extremely fine microstructure, which together with the finely tuned ferrite, bainite and martensite contents and precipitation hardening produce a particularly attractive combination of high strength and wear resistance with good cold formability and weldability.

4.1.1.1 Use

The considered steels are designed especially for manufacturing low-weight cold-formed automotive components e.g. door impact beams, body reinforcements, profiles, etc..

4.1.1.2 Chemical composition

CP-W steels are fully killed fine-grain structural steels with minimum aluminium contents of 0,015%.

Table 1

C	Si	Mn	P	S	Nb	Ti	Cr	Mo
≤ 0,18	≤ 0,8	≤ 2,2	≤ 0,025	≤ 0,01	≤0,08	≤0,18	≤ 0,60	≤ 0,40

4.1.1.3 Mechanical properties (at room temperature)

In the following table the mechanical properties of the steel tested by the producer are summarized:

Table 2

Minimum yield strength MPa	Tensile strength MPa	Minimum elongation (in %) L_0 = 80 mm	Minimum elongation (in %) L_0 = 5,65mm
700	880-1050	10	12

4.1.2 MS-W 1200 martensite phase steel

The MS-W1200 is high-strength hot-rolled strip steel with ultimate tensile strength between 1000 and 1200 MPa in the thermomechanically treated condition. Due to its chemical composition and microstructure and finely tuned microstructure of ferrite and martensite this steel display good cold forming and welding properties along with high strength and wear resistance.

4.1.2.1 Use

The considered steels are designed especially for manufacturing low-weight cold-formed automotive components such as door impact beams and body reinforcements, and of wear-exposed parts in transport vehicles and agricultural equipment.

4.1.2.2 Chemical composition

MS-W steels are fully killed fine-grain structural steels with minimum aluminium contents of 0,015%. For nitrogen fixation Ti and B may be used singly or in combination at manufacture’s discretion.

Table 3

C	Mn	Si	P	S1)
≤ 0,18	≤ 2,0	≤ 1,0	≤ 0,020	≤ 0,020

4.1.2.3 Mechanical properties (at room temperature)

In the following table the mechanical properties of the steel tested by the producer are summarized:

Table 4

Minimum yield strength MPa	Tensile strength MPa	Minimum elongation (in %) L_0 = 80 mm	Minimum elongation (in %) L_0 = 5,65mm
900	1200-1400	5	8

4.2 Lubricants

Lubricants are substances with the objective of reducing friction between moving surfaces. There are a lot of kinds of lubricants and they can be divided in oil-based and dry lubricants. Nowadays the dry lubricants are gaining a more important role because of the reduction of requirements for cleanliness, disposal and furthermore:

- they are temperature stable
- they permit a uniform distribution
- they are compatible with assembly operations (welding, bonding, clenching and riveting)
- they are more environmentally compatible than petroleum-based wet lubricants

Their limits are:

- no cooling effect
- difficulties in removing deposits of metal debris that may be left on the die surface
- there could be a premature removal from the lubricated surface and it could be difficult to replace it

As a consequence of their properties the dry lubricants are usually adopted when the lubricated points are not accessible (presence of toxic gas or the components work in vacuum) and when the temperatures are too high.
The lubrication mechanism can be intended as the interposition between the asperities of a material that guarantees a low value of shear stress. In order to have a good lubrication effect it is needed that the dry lubricants can stick together with the two surfaces or at least with one.
In this study two different dry lubricants are investigated, graphite and boron nitride and their temperature behavior is also compared with the no lubricant condition.
The lubricating properties of these dry lubes are due to their physic and chemical structure.

4.2.1 Graphite

The graphite lubricant used in the test is an aerosol with commercial name “Graphite 33” produced by “Kontankt kemier”.

Figure 12 used graphite

Graphite has a layered planar structure and in every plane the carbon atoms are bound throw covalent bonds, whereas the layers are held together by weak van der Waals forces and so they can easily slide between them. During the sliding the graphite´s particle, that initially were stick to one surface, move to the other surface and the graphite´s plane align to the direction of sliding. This effect is pronounced in case of ferrous alloys.

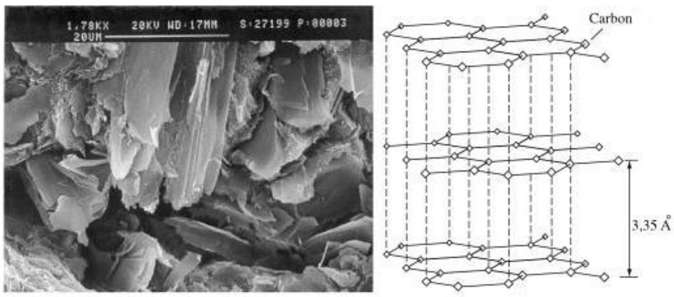

Figure 13 Graphite structure

4.2.2 Boron nitride

The boron nitride lubricant used in the test is an aerosol with commercial name “EKamold® EP” produced by “Esk”.

Figure 14 Boron nitride used

It is a spray in an ethanol based boron nitride coating, incorporating hexagonal boron nitride together with refractory binders which ensure good adhesion properties at high temperatures. Boron nitride is produced in amorphous and crystalline forms. The most stable crystalline form is the hexagonal one; it has a layered structure similar to graphite. Within each layer, boron and nitrogen atoms are bound by strong covalent bonds, whereas the layers are held together by weak van der Waals forces. The interlayer “registry” of these sheets differs, however, from the pattern seen for the graphite, because the atoms are eclipsed, with boron atoms lying over and above nitrogen atoms. This registry reflects the polarity of the B-N bonds.

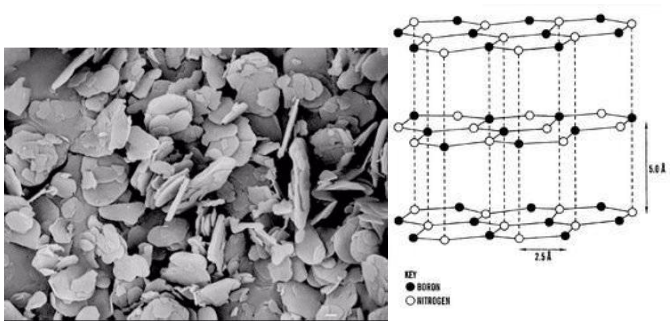

Figure 15 Boron nitride structure

4.3 Tensile test

The tensile test represents the most common test used for the evaluation of the strength-elongation characteristic of materials. This test consists in the application of a tensile state of stress to specimens with cylindrical or rectangular section by a testing equipment. In this study rectangular geometry is chosen because metal´s sheets have to be characterized. The tensile test is not the only test for the characterization of the material but it depends on the special field of application. In this investigation, the flow curves are only to be determined for low strains and for higher strains they can be accurately extrapolated so the tensile test is normally preferred for its simplicity.
The characteristics of the material at elevated temperatures are affected by the deformation speeds arising locally, in addition to the effect of temperature:

- the initial yield point drops as the temperature rises
- the initial yield point rises as the forming speed increases
- as the forming speed increases, the heat generated from forming also increases, and the rise in the initial yield point is thereby partially compensated for
- as the temperature increases, the expansion rate has an increasing effect on the material behavior
- as the temperature increases, there is often a drop in creep resistance
- elastic properties are also frequently temperature-dependent

As a consequence of the influence of the strain rate in the flow curves, the velocity of the tensile test is chosen so that the strain rate of the tensile test is similar to the strain rate of the cup deep drawing test and in particular of the flange area, where the biggest part of deformation takes place. It is not possible to choose the same strain rate because in both the case it is not constant during the process. In the flange area the strain rate varies as the radius varies and in the tensile test also it is not constant as a consequence of the constant velocity of the machine.

4.3.1 Testing equipment

The tensile tests at elevated temperature are carried out by a “Gleeble” testing machine. The specimen is heated by Joule effect and the machine is moved by a hydraulic press. In order to control the heating, as feedback loop, a thermocouple is spot welded in the middle part of a face of the specimen and in the other face the entire surface is painted with little dots for the control of the strain throws a computer vision system.

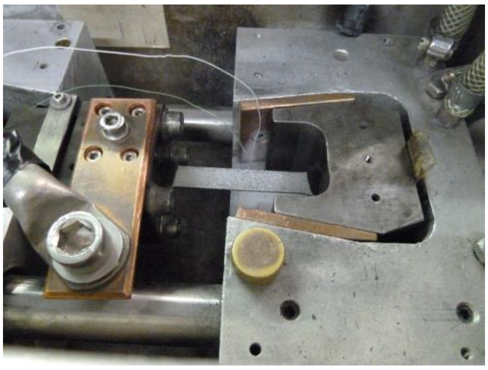

Figure 16 “Gleeble” testing machine

The tensile force is measured by a load cell and the strain of the material is measured by a camera and analyzed by “Aramis” computer vision´s software. This software evaluates the strain using the instant area of the specimen and so it is possible to calculate the real strain also after the necking. The software monitors the movement of each dot and it calculates the displacement of the dots by the selection of a starting point which is placed in a point of the specimen that doesn´t change position during the test. After the selection of the bounds of the specimen in the picture it is possible, knowing the real dimension of the specimen, to measure on a quality level each displacement. Selecting the section in which the necking occurs, the software can calculate the real strain.

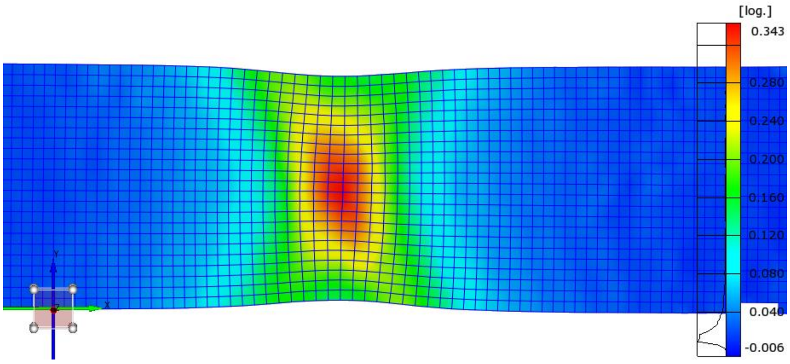

Figure 17 calculation of the real strain

4.3.2 Testing procedure

The tensile tests are conducted following the “Testing and Documentation Guideline for the

Experimental Determination of Mechanical Properties of Steel Sheets for CAE-Calculations; SEP 1240 1st Edition". For the room temperature tests, the flow curves are conducted by quasistatic tensile testing. The whole tests are executed with a constant strain rate of 0,4%/s (0,004/s) referring to the initial measuring length L. Three valid tests have to be made or more if the results show deviation of more 10%. The geometry of the specimens is summarized in the following picture:

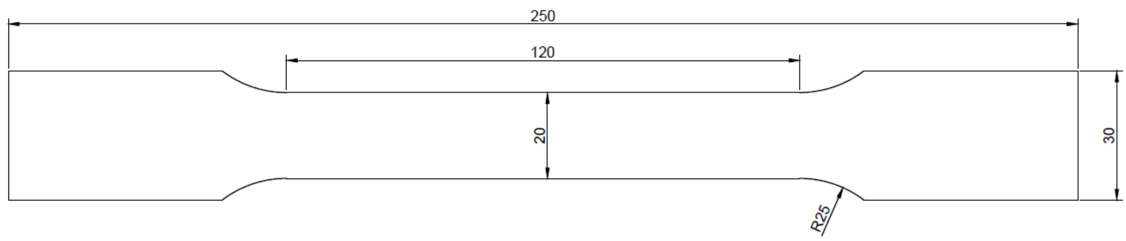

Figure 18 room temperature tensile test specimen geometry

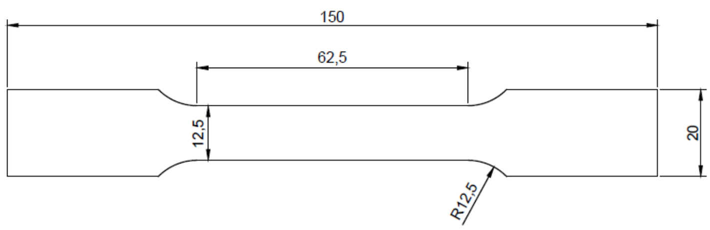

Figure 19 elevated temperature tensile test specimen geometry

In the elevated temperature tensile test the specimens is heated with a time of heating and maintenance of about 4 minutes that permit the materials to reach a uniform temperature and a uniform dark color also for the lower temperature (350°C). The uniform dark color is important to have a good color contrast with the white dots of boron nitride and only in this condition the "Aramis" software can evaluate precision displacement measurement.

The tensile tests are needed to characterize the behavior of the materials in the different conditions in which the cup deep drawing test are conducted. These tests are conducted at 400 °C, 500 °C and 600 °C and so also the tensile tests have to be conducted at least at this temperature. Three repetitions are conducted for each temperature with the same strain rate of the room temperature tensile test. Also tensile test with a strain rate very similar to the one that take place in the flange area of the cup deep drawing tests are conducted. In this case also 350 °C, 450 °C and 550 °C are tested in order to have a better understanding of the behavior of the materials and to have the possibility to characterize the cup deep drawing tests in which the transfer from the furnace to the press was not quick enough.

Testing with these two different strain rates allows the comparison of the flow curves for these different conditions.

4.3.2.1 Specimen preparation

Tensile test specimens were laser cut and milled from the laminated direction of sheet metal. Two different materials are tested: MS-W1200 and CP-W800 with thickness 1,8 mm and 1,5 mm respectively.

The zinc coating of both the materials prevents the welding of the thermocouple and the adhesion of the painted dots, so the coating is removed from both surfaces and afterwards the specimens were cleaned using acetone, in particular in the clamping zone, in order to consent a good clamp. For the painting it is used the boron nitride because the materials become dark at elevated temperature and it is possible to have a good contrast between the material and the white dots of boron nitrite that is temperature stable up to 2000 °C.

Figure 20 specimen for elevated temperature tensile test

In the room temperature tensile test the specimens do not reach a dark color like in the high temperature test. In order to have a good contrast a different way of application of the dots is used. The specimens are completely white painted and dark dots of graphite are painted in order to have a good contrast and a good quality strain acquisition.

Figure 21 specimen for room temperature tensile test

4.3.3 Evaluation of the flow curves

To calculate the force required in metal-forming processes it is necessary to know the flow curves of the metals to be formed. The flow curves are given by the flow stress as a function of strain, eliminating the elastic part of deformation.

The calculation of the yielding point and the elastic part of deformation is done using stroke and force data in output from the testing machine. The machine´s frequency of acquisition is higher than the frame rate´s acquisition of the computer vision´s system. This is due to the limited frame rate of the camera and to the limited capability of storage of the pictures. As a consequence using the machine´s data it is possible to evaluate the yielding point with higher precision and afterwards using this value to the calculation of the flow curves with the "Aramis" data.

The calculation of the plastic component of deformation is done as follows:

the stress is obtained dividing the force for the transversal area of the specimen,

$$\sigma_0 = \frac{F}{A_0} \qquad [\ 44\ ]$$

Where

$$A_0 = w_c \cdot s_0 \qquad [\ 45\ ]$$

The strain is calculated with reference to the initial specimen's length:

$$\varepsilon_0 = \frac{\Delta l}{l} \qquad [\ 46\ ]$$

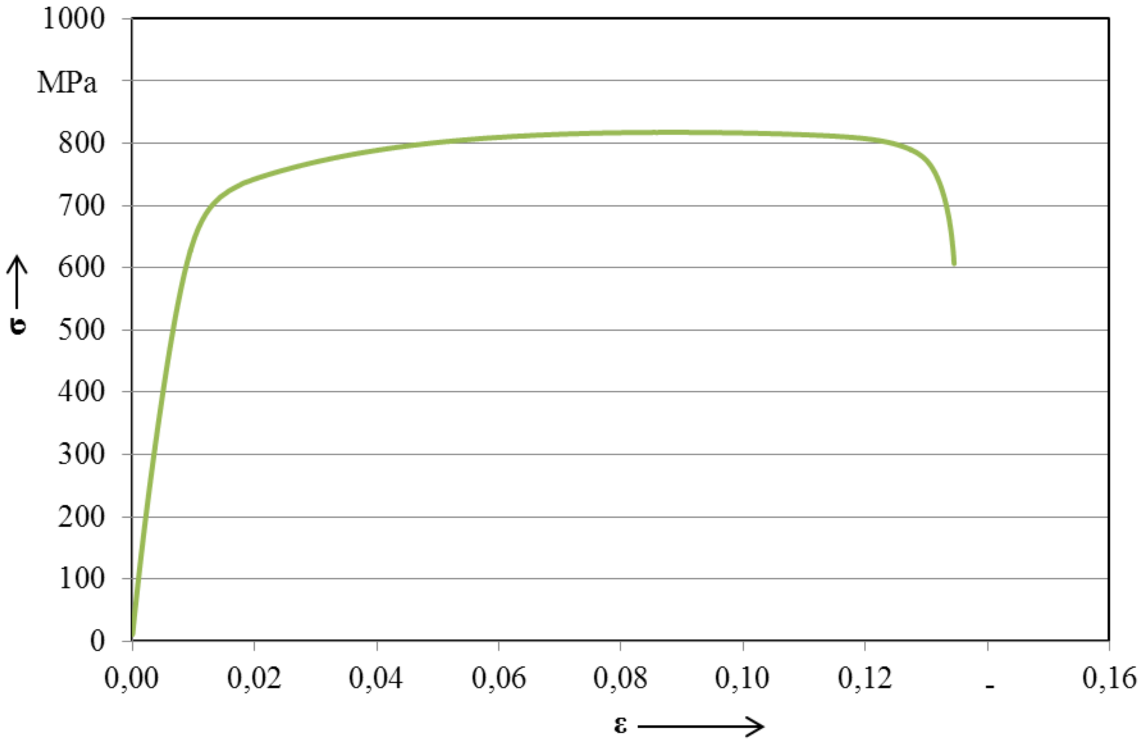

Figure 22 stress-strain curves

In these stress-strain curves it is possible to clearly identify the initial linear elastic zone and the yielding point. In order to delete the elastic component of strain a linear interpolation of the elastic part is made. After this interpolation, the tangential modulus (slope of the interpolated line) and the intercept is evaluated. It is now possible to calculate the plastic component of the strain:

$$\varepsilon_{pl} = \varepsilon_0 - \frac{\sigma_0}{tg\ modulus} - \Delta\varepsilon \qquad [\ 47\ ]$$

Where Δε is the intercept divided for the tangential modulus and with the opposite sign. The plastic part of curves and so the flow curve starts when the ε_{pl} reach values higher than 0,2%, that corresponds to a value of stress Y_s.

The curves calculated reach a maximum point and then the stress decrease. This behavior is due to the fact that the transversal section of the specimen doesn´t remains the same as before the necking occurs. The ultimate tensile stress is calculated as follows:

$$UTS = \frac{F_{max}}{A_0} \qquad [48]$$

As a consequence the points after the maximum should be neglected.

Using the true strain φ, calculated with the optical system, it is not necessary to delete the data after the ultimate tensile stress because the stress are calculated with the actual transversal area and so the stress are true stress. It is now possible to calculate the flow curve with the following operations: neglecting the points with stresses minor Y_s and normalizing the true strain so that it starts from zero.

4.3.3.1 Flow curves interpolation

After the evaluation of the flow curves, they were interpolated with different models and then it was selected the one with the lower error. The following models were considered:

Table 5 Flow curves interpolation´s formula

Gosh	$k_f = c + b(a+\varphi)^d$	
Ludwik	$k_f = b + a \cdot \varphi^c$	with b=K_{f0}
Hockett-Sherby	$k_f = b - (b-a)exp^{-c\cdot\varphi^d}$	with b=K_{f0}
Swift	$k_f = b \cdot (a+\varphi)^c$	
Voce	$k_f = b - (b-a)exp^{-c\cdot\varphi}$	with b=K_{f0}
Hollomon	$k_f = a \cdot \varphi^b$	
Swift-Voce	$k_f = a \cdot k_{f\,swift}(\varphi) + (1-a) \cdot k_{f\,voce}(\varphi)$	
Swift-Hockett-Sherby	$k_f = a \cdot (b+\varphi)^c + d \cdot exp^{(-e\cdot\varphi^f)}$	
El-Magd	$k_f = a \cdot (b+\varphi) + c \cdot (1 - exp^{-d\cdot\varphi})$	
Voce generalized	$k_f = a + (b + c \cdot \varphi) \cdot (1 - exp^{-d\cdot\varphi})$	
Bergström	$k_f = a + b \cdot \left(c \cdot (d+\varphi) + \left(1 - exp^{-e\cdot(d+\varphi)}\right)\right)^f$	
LS-Dyna	$k_f = a + b \cdot (1 - exp^{-c\cdot\varphi}) + d \cdot (1 - exp^{-e\cdot\varphi})$	with b=K_{f0}

4.4 Cup deep drawing tests

Cup deep drawing is a test by which a cylindrical blank is formed into a cup shape. The punch force reaches a maximum when $D_{f,max} \approx 0{,}77\ D_0$ and by means of a numerical simulation or the theoretical equation of Siebel based on the plasticity theory, it is possible to calculate the contribution of the friction and as a consequence to evaluate the friction coefficient.

4.4.1 Testing equipment

Cup deep drawing tests are conducted in a hydraulic press with press force of 1000 kN and maximum ram speed of 50 mm/s.

Figure 23 hydraulic press

The punch, the blank holder and the die can be heated by heating cartridges up to 400 °C.

Figure 24 heating tools

In order to reach the testing temperature up to 600 °C, the specimens were heated in an external furnace calibrated at a temperature that consent to compensate the air cooling due to the transfer to the press. After the heating indeed the specimens are manually placed over the blank holder and a very thin ring is used to center accurately the metal sheet with the punch and the die. Afterwards the matrix, which is connected with an upper ram, goes in contact with the specimen and they precede the movement together with the blank holder applying a constant force during the process that is measured by three load cells. The force of the stationary punch is measured by one load cell. The load cells are equipped with a cooling system in order to have accurately measurement also if the components are heated.

The specimens consist in round blanks with diameter of 90 mm laser cut from steel sheet of MS-W1200 and CP-W800 respectively 1,8 mm and 1,5 mm thickness. The punch has a diameter of 50 mm and as a consequence the drawing ratio is 1,8. The drawing depth is chosen in relation to the stroke that corresponds to the maximum punch force and in particular three drawing depth is performed: one above the maximum, one below the maximum and the last one correspondent as possible to the maximum. The blank holder force and the ram speed are chosen as a function of the maximum that the machine permits.

Figure 25 different drawing depth specimen

In order to avoid failure it is evaluated the geometrical dimension of all the components, and in particular the die clearance that is determined from the following empirical equation:

$u_D = s_0 + 0{,}07\sqrt{10 \cdot s_0}$ for steel sheet

$u_D = s_0 + 0{,}02\sqrt{10 \cdot s_0}$ for aluminum sheet

$u_D = s_0 + 0{,}04\sqrt{10 \cdot s_0}$ for other nonferrous metals

$u_D = s_0 + 0{,}20\sqrt{10 \cdot s_0}$ for high-temperature alloys

(Lange, Handbook of Metal Forming, 1975)

As a consequence of the unavoidable thickness variations during the process, the selection of an accurate clearance is a significant problem. It does not have to be too large to form a true cylinder and it doesn´t have to be too small to avoid ironing and danger of cracking.

The die and punch radii have an important role in the process. If the die radius is too small the drawing load and the limiting drawing ratio increase, on the other hand large radius reduces the contact area between the blank holder and the flange and increases the possibility to form wrinkles. It has to be chosen depending on the size and thickness of the specimen. In this study the minimum die radius is calculated with the following empirical equation:

$$r_D = 0{,}035 \cdot [50 + (D_0 - d_P)]\sqrt{s_0} \qquad [\,49\,]$$

The factor 0,035 can be increased to 0,08.

The punch radius has to be larger than the die radius to avoid piercing the specimen.

All geometrical dimensions are summarized in the following table:

Table 6

Material	D_0 [mm]	t_0 [mm]	d_m [mm]	d_p [mm]	u_d [mm]	r_d [mm]	r_p [mm]
MS-W1200	90	1,8	56	50	3	5	10
CP-W800	90	1,5	56	50	3	5	10

In this study two different lubricants were tested, graphite and boron nitride. Both lubricants were sprayed on the specimens in a uniform thin coating that consent to cover the complete surface. The quantity of lubricants is measured weighting the specimens before and after the lubricant application by a digital balance with 1/100g resolution. The results of the balancing are summarized in the following table:

Table 7 Lubricant´s quantity

Lubricant	Lubricant´s quantity [g/m^2]	Error [g/m^2]
Graphite	7,12	2,84
Boron nitride	8,38	2,49

Figure 26 graphite coated specimen

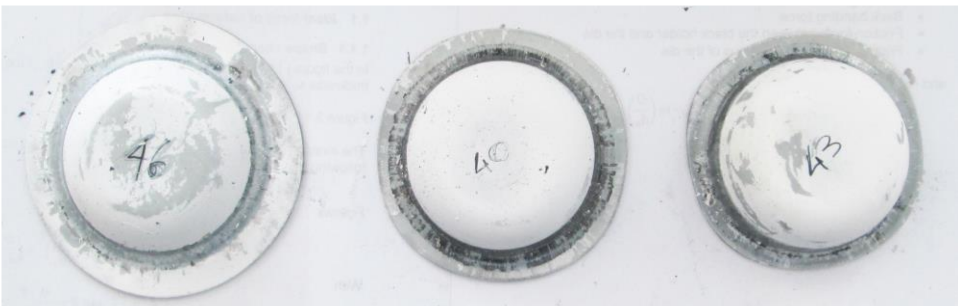

Figure 27 boron nitride coated specimen

4.4.2 Testing procedure

The testing parameters are chosen from practical stamping operations.

The blank holder force is calculated in order to avoid wrinkling and the following empirical equation is used for the estimation:

$$p_{bh} = 0.002 \cdots 0.0025 \cdot \left[(\beta_0^2 - 1)^3 - 0.5 \cdot \left(\frac{d_p}{100 \cdot s_0}\right)\right] \cdot R_m \qquad [\ 50\ ]$$

The blank holder force is calculated as follows:

$$F_{bh} = \frac{\pi}{4} \cdot (D_0^2 - d_d^2) \cdot p_{bh} = \frac{\pi}{4} \cdot d_p^2 \cdot (\beta_0^2 - 1) \cdot p_{bh} \qquad [\ 51\ ]$$

The maximum stroke is calculated approximately with the volume conservation respectively in the flange area and in the wall area:

$$stroke = \frac{(D_0^2 - D^2)}{4 \cdot \left(d_p + \frac{s_0}{2}\right)} \qquad [\ 52\ ]$$

The drawing ratio is a consequence of the diameter of the specimen and the diameter of the punch.

The room temperature´s parameters of the test are summarized in the following table:

Table 8 Room temperature cup deep drawing parameters

BHF [kN]	Velocity [mm/s]	β_0
30	27	1,8

At elevated temperature the tests conducted with this parameter failed, so the blank holder force and the ram velocity were decreased. The elevated temperature parameters of the test are summarized in the following table:

Table 9 elevated temperature cup deep drawing parameters

BHF [kN]	Velocity [mm/s]	β_0
18	18	1,8

For both materials the tests are conduct without lubricant, with graphite and with boron nitride and for every kind of coating three different temperatures (400 °C, 500 °C and 600 °C) are tested. In order to optimize the number of available specimens, three repetitions are made with drawing depths above the maximum punch force and with drawing depth correspondent the maximum punch, for the drawing depth below the maximum force two tests are made.

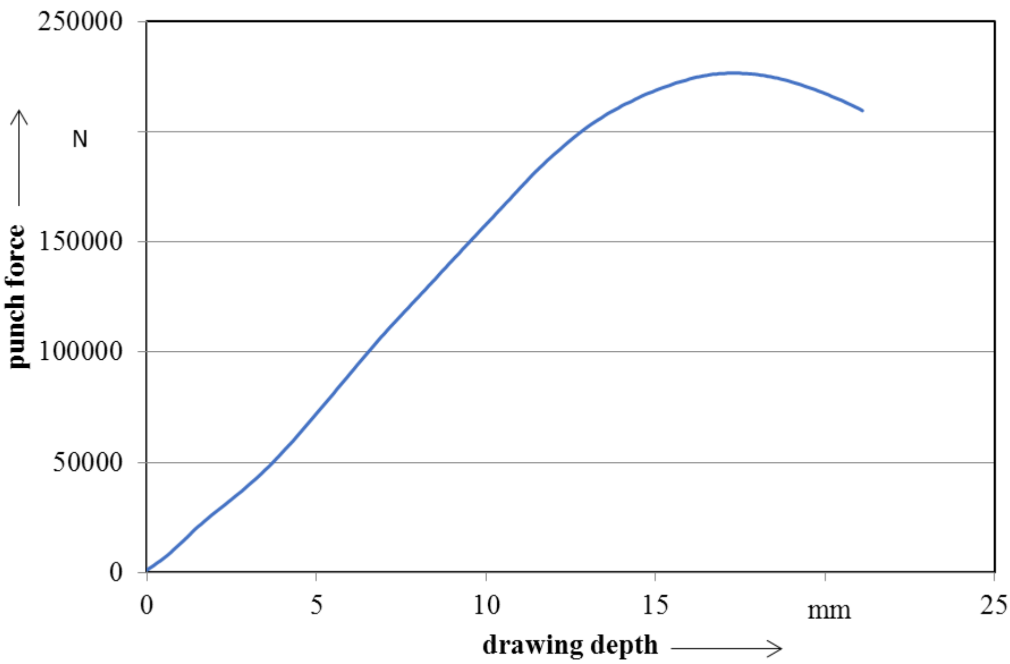

Figure 28 punch force in cup deep drawing test

After every test the external diameter of the flange area of the specimens is measured with a digital caliber in four different directions and the mean value and the standard deviation is calculated. It was necessary to calculate the diameter in four different directions to filter the earing effect of the anisotropy.

The measured diameters as function of the drawing depth are fit with a second degree polynomial.

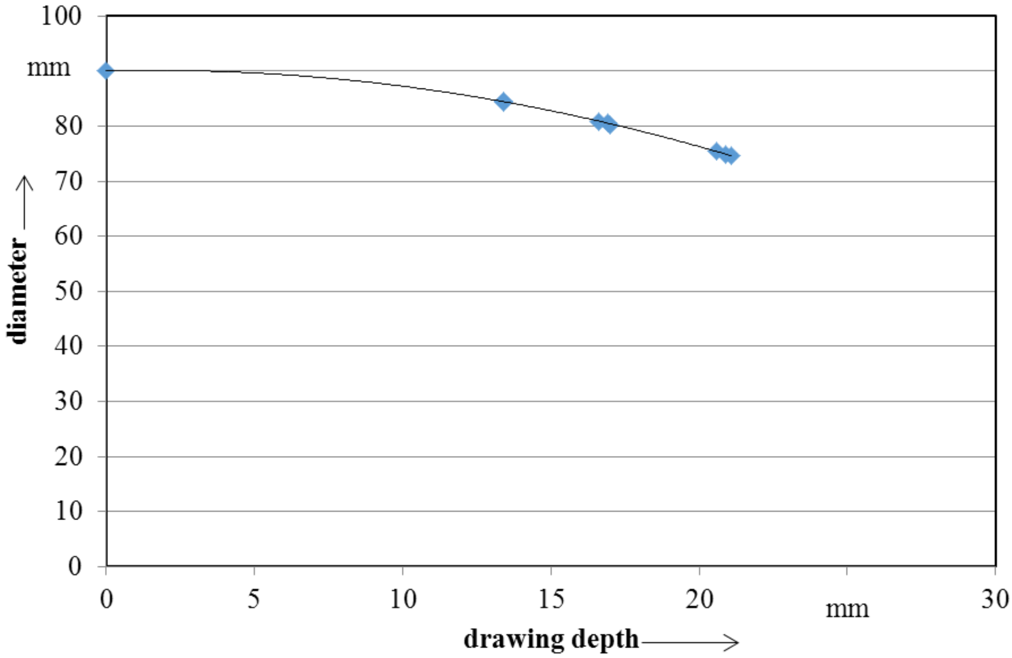

Figure 29 external diameter

5 Calculation of friction coefficient

The theoretical maximum punch force during the process can be calculated by means of numerical simulation or analytical equation. Matching these results with the experiments it is possible to evaluate the friction coefficient that is used as variable in the calculation.

5.1 Numerical simulation and identification

Nowadays the numerical simulation has a very important role in the production of components because it permits to evaluate the metal flow during process. So it is possible to choose the suitable parameters and their influence in process in order to reach a quality product and avoid failures.

The numerical simulations show good agreements with the experimental results but in any case they have to be validated and so a comparison with the experiments is necessary. The cup deep drawing is a good validation test as a consequence of the facility in the parameter control and on the easily predictable metal flow. It is an axisymmetric process and so the material flows in the same way in any direction assuming an isotropic behavior of the material therefore a 2D simulation can be conducted with good results. Additional simplifications on the simulations are the temperature dependent material properties. The temperature effect is considered only in the change of flow curves of the materials and the increase of temperature to the blank deformation is neglected.

In this investigation, finite element analysis of cup deep drawing tests are carried out to evaluate the friction coefficient and compared with the result of the analytical formula of Siebel.

The complete description of the creation of the model used in this simulation is described in the following part and also a summary of the assumption and simplification that are necessary to model the process is explained.

5.1.1 Assumption made in this simulation

The numerical simulation is conducted with the following simplifications:

- The materials are considered isotropic (elevated temperature)
- The temperature is assumed constant during the process
- The mechanical interactions between the contact surfaces is assumed to be the

frictional contact

- For shells and membranes, the thickness change is calculated from the assumption of incompressible deformation of the material
- It is assumed that no reverse loading occurs during simulations and so the Buchinger effect is not modeled.
- Quasi-static process

5.1.2 Part definition and assembly

The deformable blank is represented by a deformable solid part with a planar shell base feature.

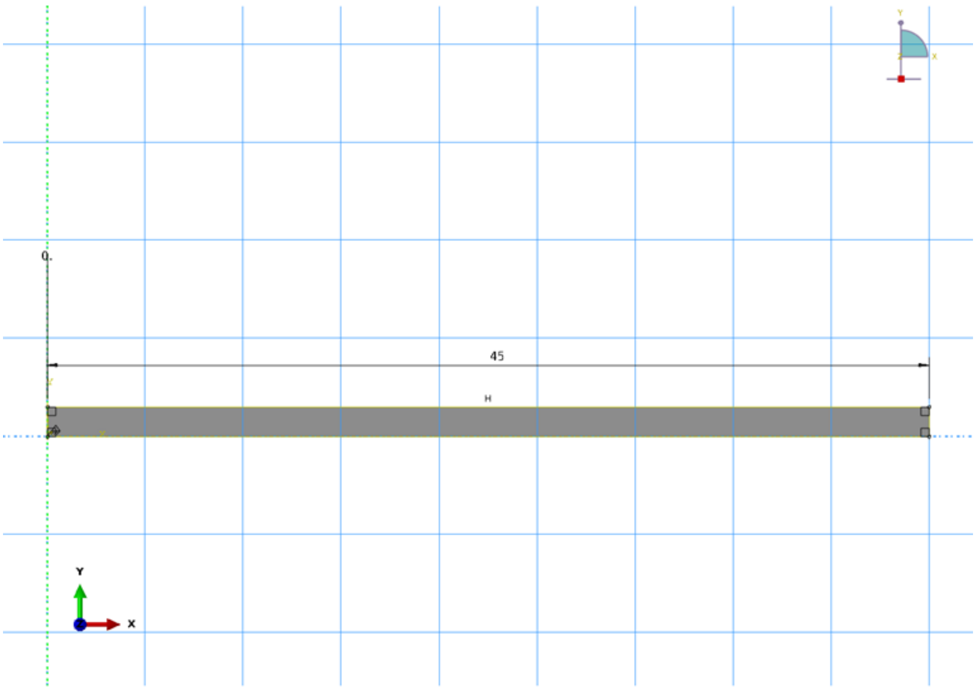

Figure 30 part definition

The die, the punch and the blank holder are represented as analytical rigid body because they are stiffer than the blank. After they were created, a reference point for every solid object is defined. In any part the center of the arc is used as reference point.

Once every part is defined, they are assembled all together with respect of the geometry used in the experimental tests and focusing on edge to edge contact in any interface between the blank and the other components.

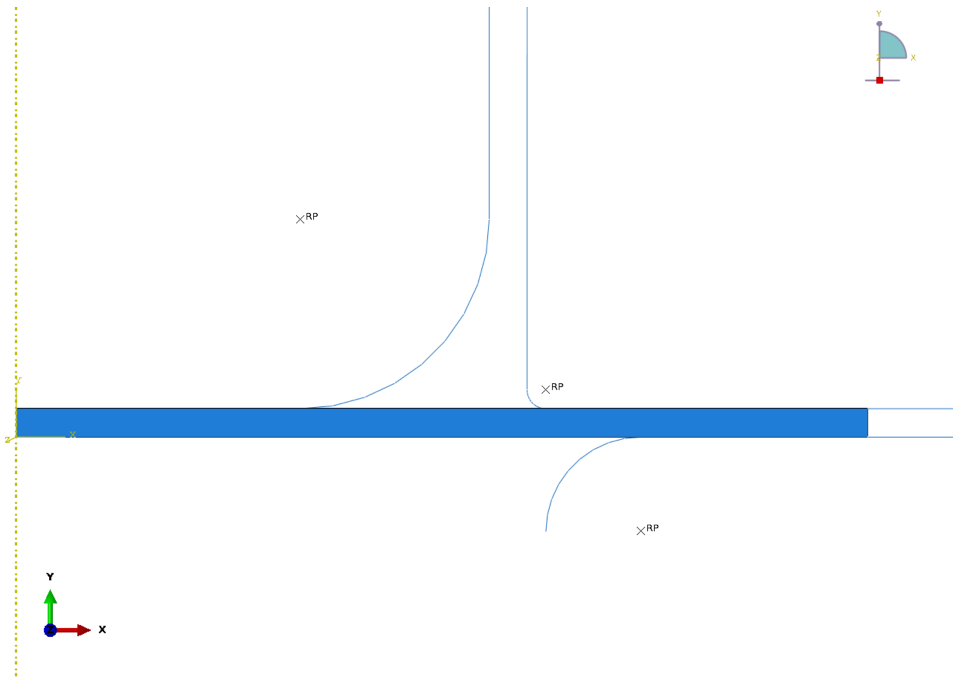

Figure 31 part assembly

5.1.3 Material and section properties

The materials utilized in this simulation are the high strength steels CP-W800 and MS-W1200. The elastic properties of both materials are characterized by a Young´s modulus value of 210 GPa and a Poisson´s ratio of 0,3. The inelastic strain-stress behavior of the materials was calculated by the tensile tests. The problem of the temperature dependent stain-stress behavior is overtaken by the use of different flow curves for every temperature.

The material furthermore undergoes considerable work hardening as it deforms plastically. It is likely that plastic strains will be large in this analysis; therefore, hardening data are provided up to a value of 1 of plastic strain.

5.1.4 Defining steps

The principal sources of difficulties in the simulation of contact analysis in Abaqus/Standard is due to the fact that the rigid body motion of the components before contact conditions constrain them and sudden changes in contact conditions, which lead to severe discontinuity iterations as Abaqus/Standard tries to establish the correct condition of all contact surfaces. Therefore, wherever possible, it has to take precautions to avoid these situations. The removal of rigid body motion does not present particularly difficulties. Simply it has to be ensured that there are enough constraints to prevent all rigid body motions of all the components in the model. This can be done by the use of boundary conditions to get the components initially into contact, instead of applying loads directly. Using this approach it may require more steps but the solution does not present problems.

As a consequence of the previous problems solving, the deep drawing simulation is conducted with the creation of two steps:

- The blank holder force is a controlling factor in these forming processes; therefore, it needs to be introduced as a variable load in the analysis. In this step the blank holder force is applied with the same magnitude as in the cup deep drawing tests. A quasi-static nature of the problem is given and also the nonlinear response is considered.
- In the second and final step it is imposed to the punch to move down to complete the forming operation.

5.1.5 Defining contact interactions

The model will use contact pairs instead of general contact, since general contact is not available for analytical rigid surfaces in Abaqus/Standard.

Contact is defined between the top of the blank and the punch, the top of the blank and the blank holder, and the bottom of the blank and the die. The friction coefficient is considered the same for every surface in contact and an automatic contact stabilization is created in order to alleviate convergence difficulties that may arise due to the changing contact states (in particular for contact between the punch and the blank).

5.1.6 Boundary conditions and loading for Step 1

In this step, contact is established between the blank holder and the blank while the punch and die are held fixed. The symmetric boundary condition is applied to the blank on the region on the symmetry plane. The punch and the die are constrained completely and the blank holder is constrained in order to can move only in the vertical direction.

A mechanical concentrated force is applied to the blank holder to simulate the bank holder force.

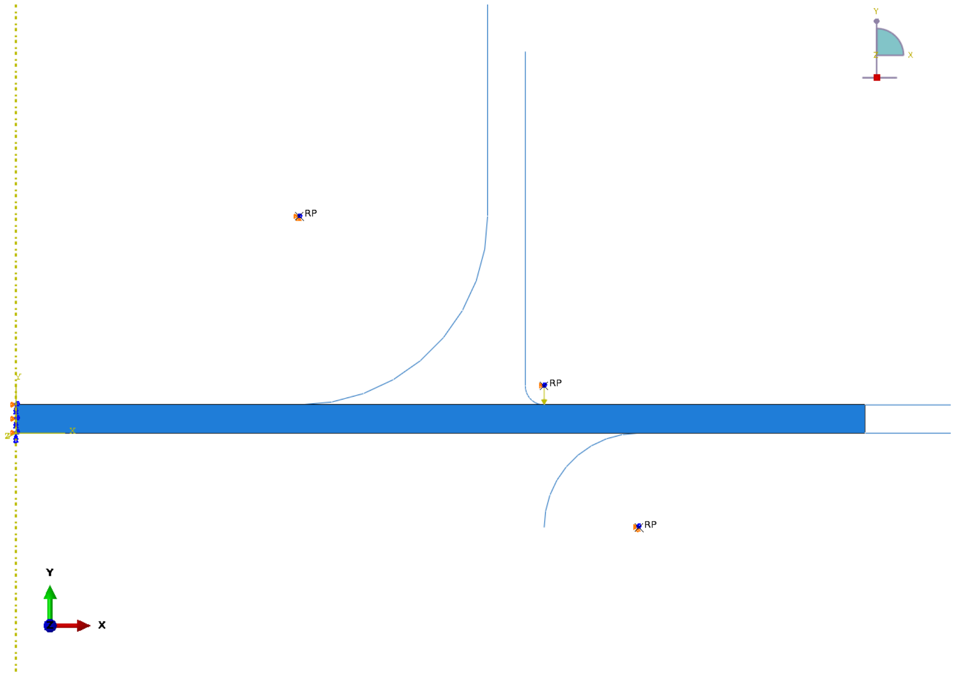

Figure 32 blank holder force boundary condition

5.1.7 Boundary conditions for Step 2

In this step the punch moves down to form the cup. A drawing depth of 25 mm is imposed to the punch as boundary condition in the vertical direction.

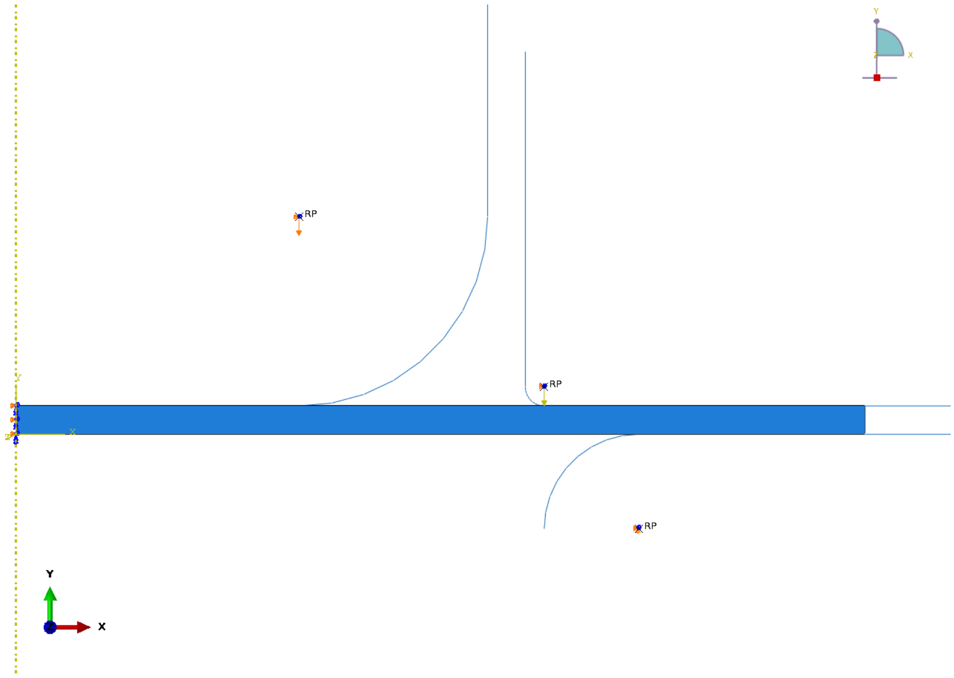

Figure 33 drawing depth boundary condition

5.1.8 Mesh creation

The type of element used in the mesh has relevant differences in the results of the numerical simulation. As a consequence the element has to be chosen before the design of the mesh.
Several aspects of the model have to be considered such as the geometry of the model, the type of deformation, the applied loads. In the deep drawing simulation the following points have to be considered:

- First-order elements (with the exception of tetrahedral elements) should be used for contact simulations. When using tetrahedral elements, modified second-order tetrahedral elements should be used for contact simulations.
- Significant bending of the blank is expected under the applied loading. Fully integrated first-order elements exhibit shear locking when subjected to bending deformation. Therefore, either reduced-integration or incompatible mode elements should be used.

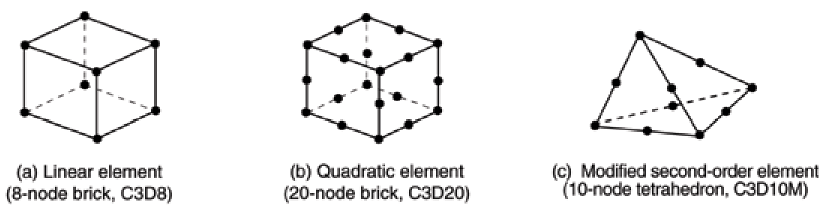

Figure 34 mesh type

The meshing of the blank is made with the element CAX4R, which is a four node bilinear axisymmetric quadrilateral element with reduction integration. The material model used is the isotropic Von Mises hardening rule.
Along the horizontal edges of the blank 90 elements are specified and 8 elements along each vertical edge of the blank. The tools are modeled with analytical rigid surfaces so they need not be meshed

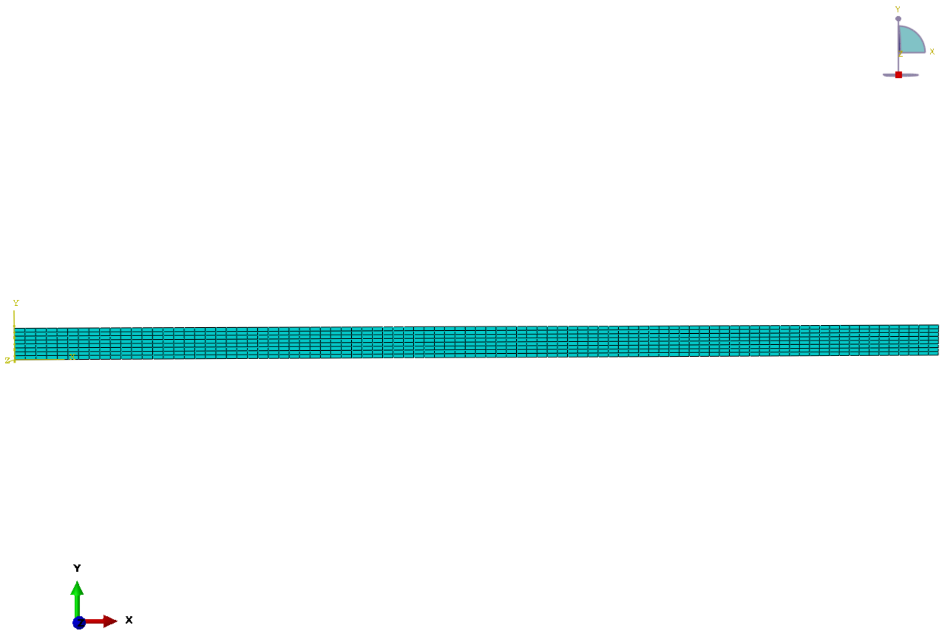

Figure 35 component meshing

5.1.9 Postprocessing

After the computation is done, it is possible to view the deform shape of the blank to have a qualitative confirmation of the good model of the real process.

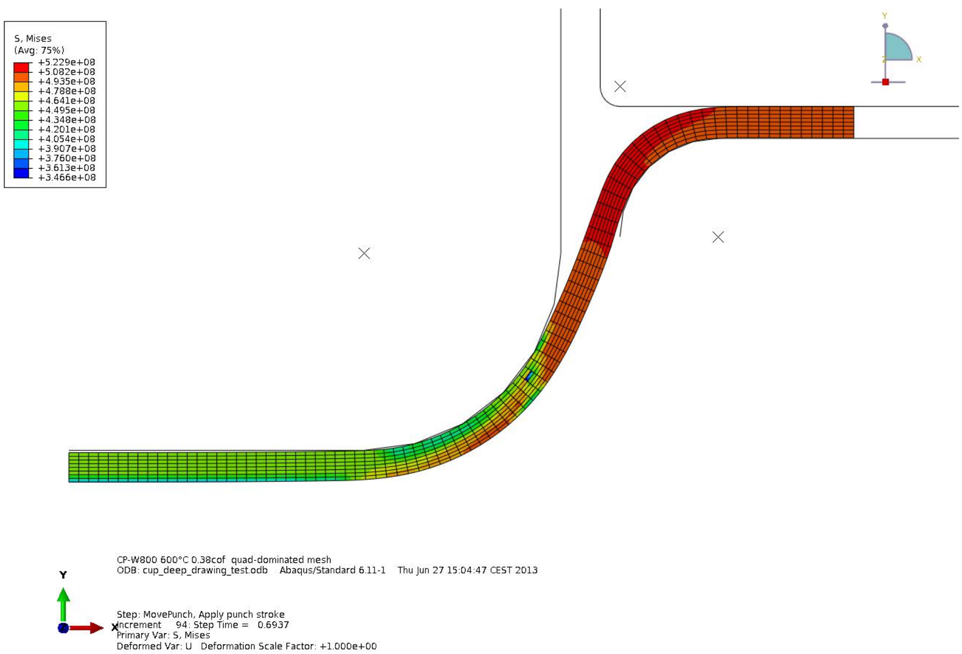

Figure 36 deformed shape at maximum drawing load

If the contact between the blank and both the die and blank holder is not maintained, it can be due to the fact that the blank holder force is not enough.

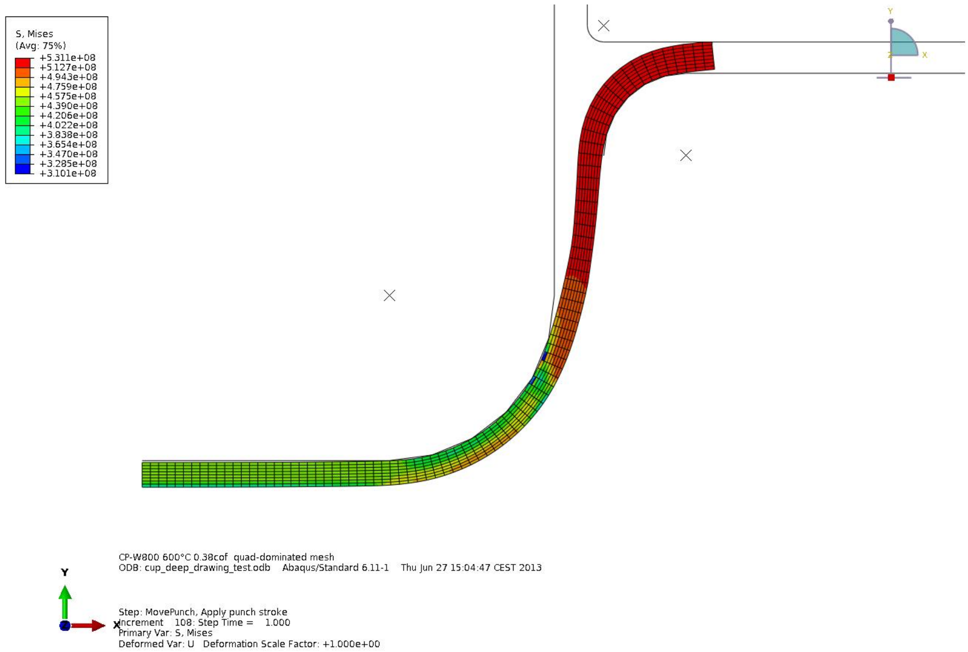

Figure 37 deformed shape at maximum drawing depth

At elevated temperature the friction coefficient reaches high value which combined with the low strength at this temperature have the consequence to stress the material during the formation of the cup. In the punch radii in particular the material is subjected to a state of stress that is not correctly modeled with the rectangular mesh because the thickness collapse in a point in this region and the results of the simulation are not accurate.

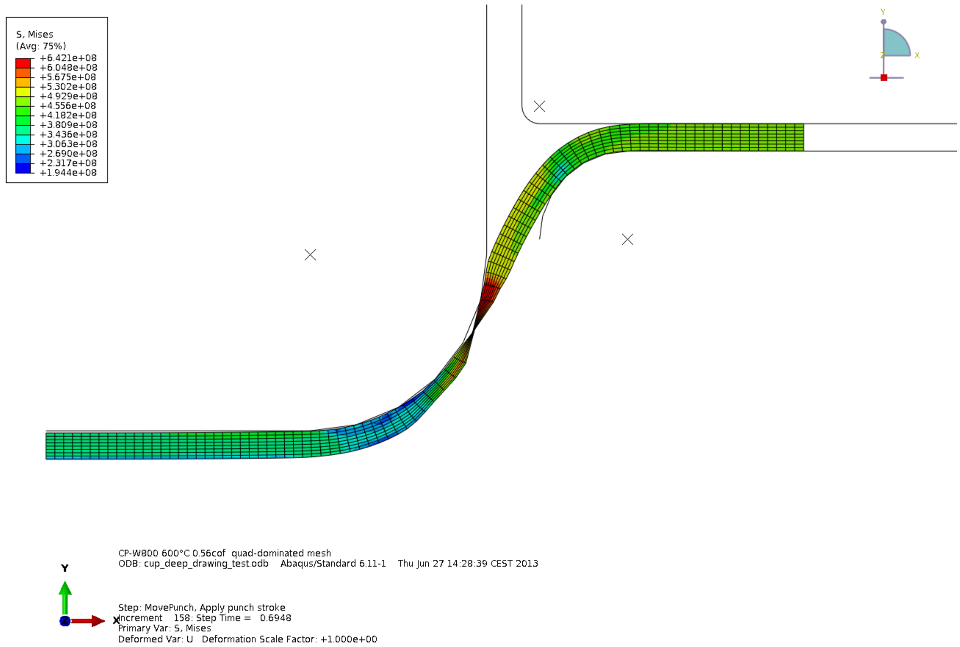

Figure 38 numerical simulation failure

It is needed to use a triangular mesh that consent to avoid this problem and model correctly the behavior of the material during the process for that combination of temperature and friction coefficient.

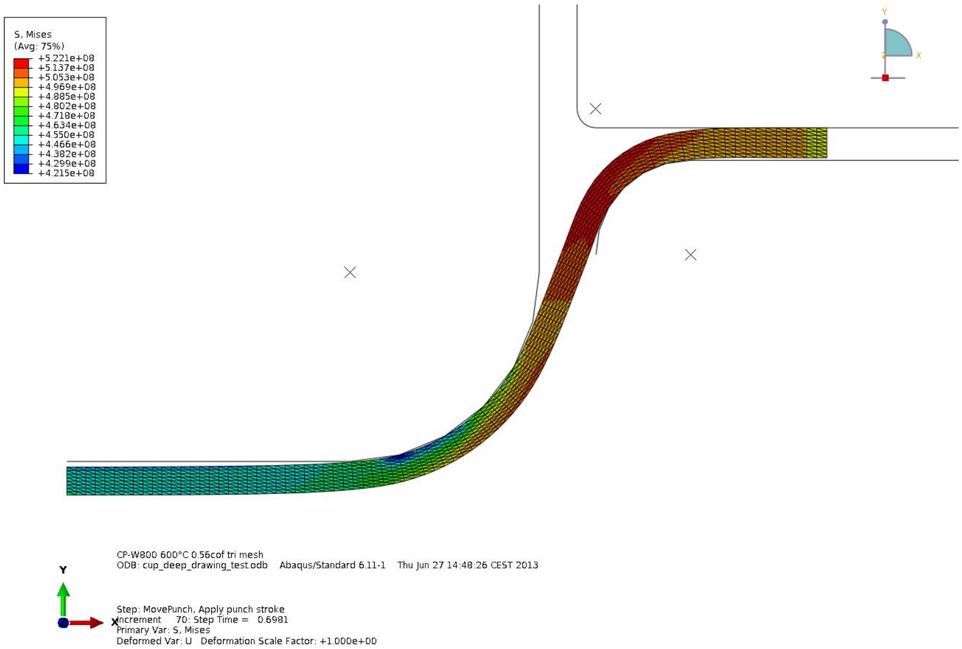

Figure 39 triangular mesh

5.2 Siebel´s formula application

In order to calculate the friction coefficient by means of the Siebel´s formula, the following parameters have to be used:

5.2.1 Geometric parameters

- d_0 initial piece diameter
- t_0 thickness of the sheet
- r_d die radii

5.2.2 Forces

The punch force is the force measured by the load cell of the punch during the process.

5.2.3 Instantaneous blank diameter D

For the evaluation of the instantaneous blank diameter D three different drawing depth tests are conducted: drawing depth above the maximum punch force, drawing depth below the maximum and drawing depth as equal as possible to the maximal punch force. The flange area of every test is measured in four different directions in order to neglect the variation due to the anisotropy and the measured diameters are interpolated as a function of the drawing depth with a second order polynomial. Using the calculated formula it is possible to calculate the diameter corresponding to the maximum punch force.

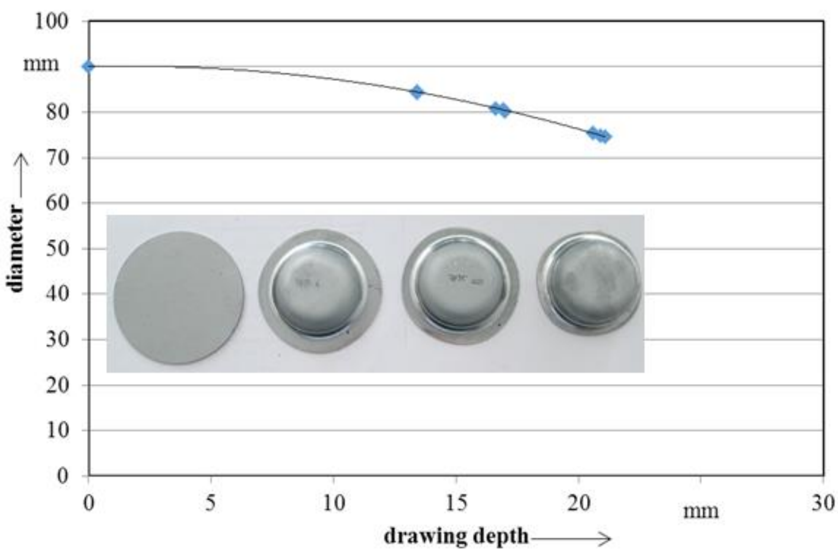

Figure 40 different drawing depth

5.2.4 Blank holder force F_{fh}

The blank holder force F_{fh} is constant during the process; it is measured by three load cells.

5.2.5 Flow stress k_{fmI}

The flow stress K_{fmI} can be calculated as the arithmetic average of the flow stress in the outer and inner:

$$k_{fmI} = \frac{1}{2}\left(k_{f1} + k_{f2}\right) \qquad [\,53\,]$$

k_{f1} and k_{f2} are calculated with φ_1 φ_2.

5.2.6 Flow stress k_{fmII}

In the bending zone, the central fiber of the cross section is the no lengthened fiber so the strain is calculated referring to it.

The longitudinal strain ε_x of a fiber, calculated as change in length referred to the unbend length is

$$\varepsilon_x = \frac{\Delta l}{l} = \frac{(r_u+y)\alpha - l_0}{l_0} \qquad [\,54\,]$$

where α is the bend angle $\alpha=l_0/r_u$, r_u is the radius of bending and y the distance from the center. Therefore it follows:

$$\varepsilon_x = \frac{y}{r_u} \qquad [\,55\,]$$

Since the neutral line has a radius $r_u=r_d+s_0\backslash 2$, the strains for the edge are:

$$\varepsilon_{x,external} = -\varepsilon_{x,internal} = \frac{s_0}{2r_u} = \frac{s_0}{2r_d+s_0} \qquad [\,56\,]$$

As a consequence of the linear strain distribution across the sheet thickness, the average bending strain $\bar{\varepsilon}$ is given by

$$\bar{\varepsilon} = \frac{\varepsilon_x}{2} \qquad [\ 57\ ]$$

The workpiece undergoes twofold bending in the region of the die radius so that the total average bending strain after unbending is

$$\bar{\varepsilon}_{tot} = 2\bar{\varepsilon} = \varepsilon_x \qquad [\ 58\ ]$$

The corresponding true strain is given by

$$\varphi_b = ln(1 + \bar{\varepsilon}_{tot}) \qquad [\ 59\ ]$$

Using this result, the strain after the bending can be determined adding to this strain the true strain calculated after the shape changes in the flange area:

$$\varphi_3 = \varphi_2 + \varphi_b \qquad [\ 60\ ]$$

Calculating the arithmetical average value follows:

$$\varphi_{k_{fmII}} = \frac{\varphi_2 + \varphi_3}{2} \qquad [\ 61\ ]$$

5.2.7 Calculation

In the experiments conducted in this investigation the formula of Siebel cannot be utilized as it is presented because it includes some approximations that influence the results.

The equation considers a complete cylindrical shape of the cup but in the real process the die radii, the punch radii and in particular the die clearance implicates a non-vertical inclination of the wall of the cup. As a consequence the blank is not bended 90° but the bending angle change as the drawing depth increase. This angle is calculated for every different test using the drawing depth that corresponds to the maximum punch force, the die clearance and the contributions of the die and punch radii.

The influence of considering this factor in the calculation of the punch force with the Siebel´s formula correspond in the change of angle for the computation of the contribute due to the friction at the die radii and in the fact that the force calculate from the stress of the material in the wall of the cup is not directly in the same direction of the motion of the punch but has to be multiply for the sin of the angle in order to calculate the component of the force that correspond to the vertical direction.

In addition to this fact the average diameter utilized for the calculation do not correspond to the punch diameter plus a sheet thickness but correspond to average value between the punch diameter and the die diameter. Furthermore, the shape deformation in radial direction can be accurately calculated only in the flange area because as the material flows into the die, the blank is subjected to complex shape deformation that makes the calculation of the ideal force of deformation not precise.

At the end the ideal punch force results:

$$F = \pi \cdot \left(\frac{d_d + d_p}{2}\right) \cdot \sin\alpha \cdot t_0 \left[e^{\mu\alpha} \cdot \left(1{,}1 \cdot k_{fmI} \cdot \ln\left(\frac{D}{d_d}\right) + \frac{2 \cdot \mu \cdot F_{fh}}{\pi \cdot D \cdot t_0}\right) + \frac{k_{fmII} \cdot t_0}{2 \cdot \left(r_d + \frac{t_0}{2}\right)} \right] \qquad [\ 62\ ]$$

6 Results / Discussion

6.1 CP-W800

6.1.1 Experiment results

6.1.1.1 Tensile tests

The flow curves, results of the tensile test for the material CP-W800 are summarized in the following figure. The curves were extrapolated up to a strain rate value of 1. The error bar represents the standard deviation calculated between the values of the four replications conducted for every temperature.

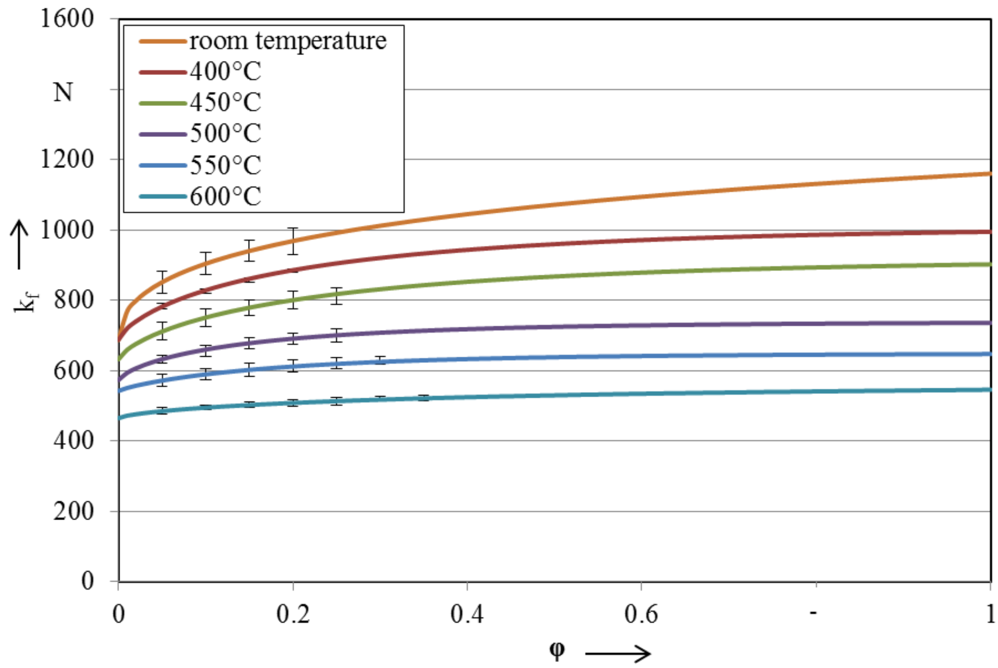

Figure 41 CP-W800 flow curves, for different temperatures

As the temperature increases, the strength needed for the deformation of the material decrease and also the elongation reaches higher values.

For this material, the temperature 350 °C is not represented because the specimens did not break in the central section that is at the highest temperature and so below 400 °C the material have the same behavior and characteristic of the room temperature.

For this material the Hockett-Sherby interpolation formula was used:

$$k_f = b - (b - a)exp^{-c \cdot \varphi^d} \qquad [\,63\,]$$

The calculated coefficients are summarized in the following table.

Table 10 CP-W800 Hockett-Sherby coefficients

Hockett-Sherby	**a**	**b**	**c**	**d**	**e**	**f**
room temperature	679	1490	0,90	0,442	-	-
350°C	711	940	7,41	0,820	-	-
400°C	688	1009	3,11	0,732	-	-
450°C	632	919	2,86	0,727	-	-
500°C	574	739	4,13	0,745	-	-
550°C	543	649	4,18	0,854	-	-
600°C	465	563	1,75	0,680	-	-

6.1.1.1.1 Influence of strain rate

The flow curve change due to the higher strain rate is not the same for all the temperatures. In particular for the CP-W800 it is not possible to appreciate differences in the flow curves for low temperature (the standard deviation in every test is greater than the differences throw the tests) and only at 600 °C it is possible to see the higher strength needed for the equivalent strain.

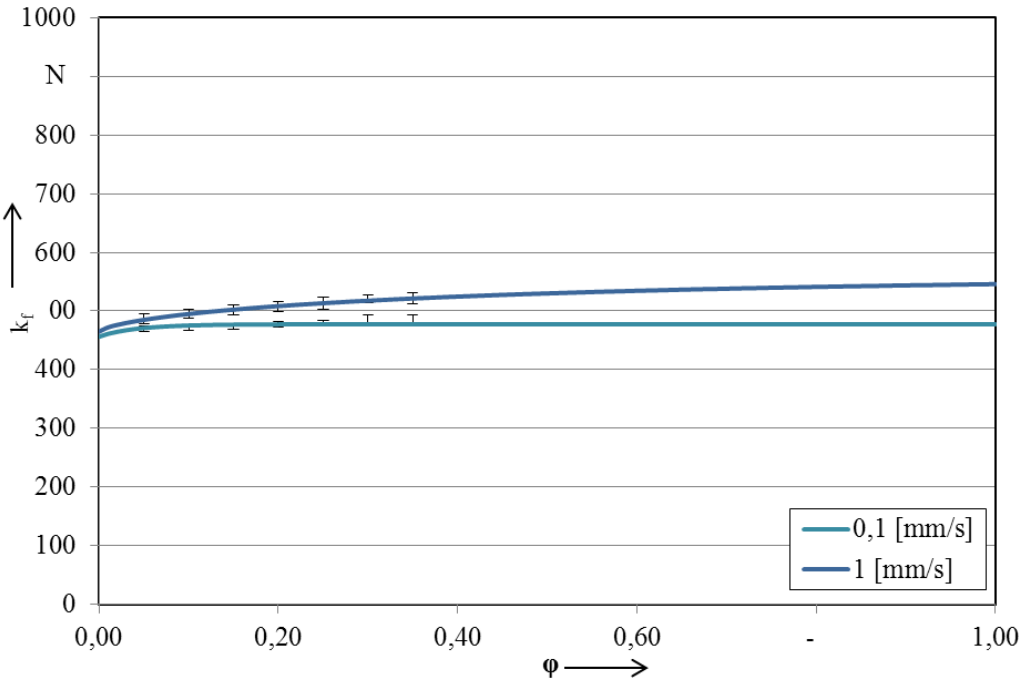

Figure 42 CP-W800 influence of the strain rate on the flow curves at 600°C

6.1.1.2 Cup deep drawing tests

The maximum force measured by the punch´s load cells can give a qualitative comparison between the different lubrication conditions. By means of this analysis it is not possible to compare the behavior of the same lubricant in different temperature condition because the punch force is not only influenced by the friction but also by the strength of the material which is not constant with the temperature. It is possible to observe that at room temperature there are not substantial differences between the different lubrication conditions. For elevated temperatures the graphite is the most performing lubricant because the punch force decreases as the temperature increases unlike in the other conditions. Without lubricant there are no big differences in the punch force as the temperature changes so the reduction in the material strength due to the temperature is compensated by the increase of friction. The boron nitride gets worse behavior also compared to no lubricant condition and the maximum force increase with the temperature. At 600 °C there are no results because all the tests failed as a consequence of the increased friction. This bad behavior of the boron nitride was evident also during the tests because for high temperature it was needed to reduce the velocity to avoid failure that didn´t occur in the tests without lubricants.

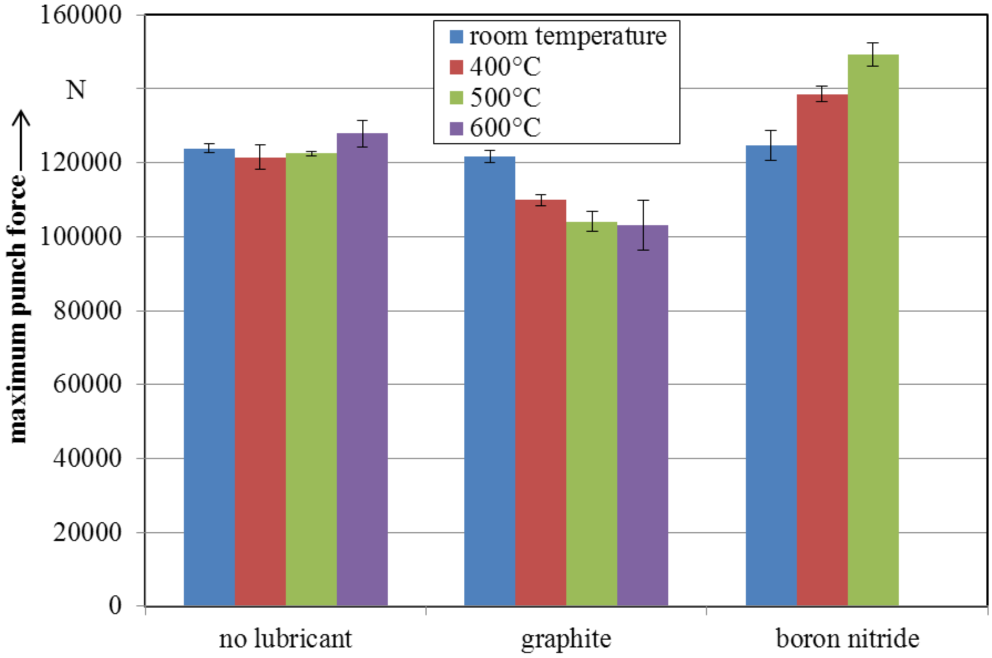

Figure 43 CP-W800 Maximum punch force sorted by lubricant

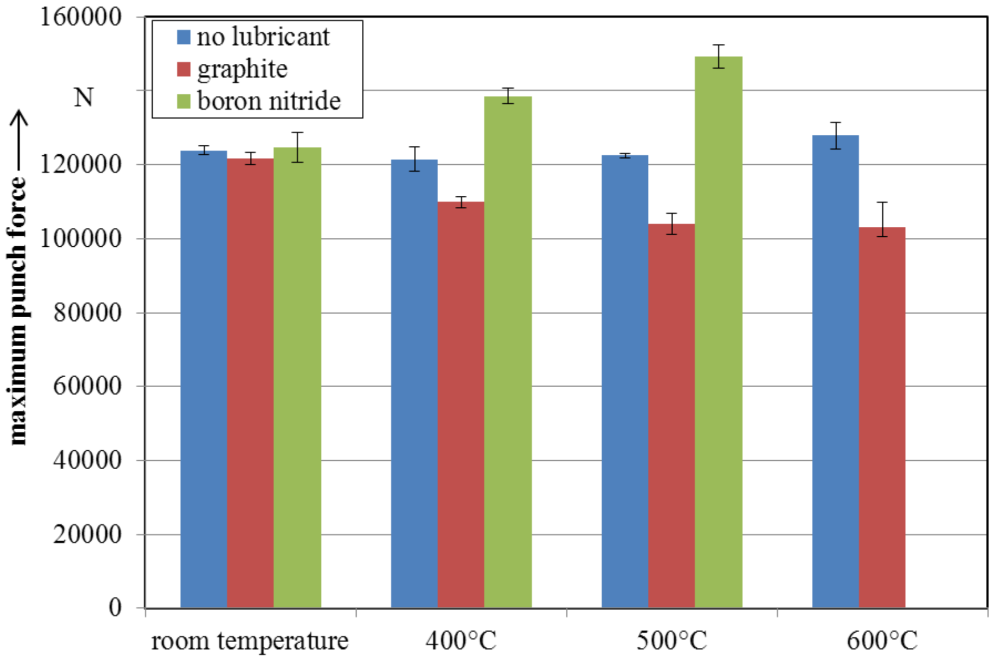

Figure 44 CP-W800 Maximum punch force sorted by temperature

In the table the test conditions and the test output are summarized, the maximum force is calculated as an average of the three tests with drawing depth above the maximum force and also the standard deviation is calculated from the same data. The diameter corresponded to the maximum punch force is calculated with the formula obtained by the interpolation of the flange diameters of the specimens as a function of the drawing depth.

Table 11 CP-W800 cup deep drawing test summary

	Lubricant	**max force [N]**	**D [mm]**	**BHF [N]**	**velocity [mm/s]**
room temperature	-	123900	79,48	32550	28
room temperature	graphite	121767	79,86	31660	27
room temperature	boron nitride	124617	78,48	31711	28
400 °C	-	121486	79,99	19615	27
400 °C	graphite	109914	79,70	18181	18
400 °C	boron nitride	138629	77,76	18328	18
500 °C	-	122500	78,91	18212	17
500 °C	graphite	104140	80,16	17917	18
500 °C	boron nitride	149220	78,73	18144	17
600 °C	-	127840	79,27	16339	17
600 °C	graphite	103117	78,65	16908	18
600 °C	boron nitride	-	-	-	-

6.1.2 Numerical calculation of friction coefficients

In this investigation the interested output is the punch force, so the reaction force in vertical direction of the punch is exported from Abaqus to a worksheet. As a consequence of the representation of the punch as analytical rigid body it cannot be meshed and so the reaction force is not computed in a node but in correspond to the reference point.

It is plotted the punch force-drawing depth graphic and the external diameter-drawing depth graphic calculated by means of the numerical simulation, in order to create this graphic the displacement of the punch and of the node in the midpoint of the thickness in the external diameter of the blank is exported. This graphics can be plotted together with the experimental data and confront with them. It is done this qualitative comparison between a condition with low friction coefficient and a condition and with a high friction coefficient:

- CP-W800
- Graphite
- Room temperature
- Friction coefficient 0,04

And

- CP-W800
- No lubricant
- 500°C
- Friction coefficient 0,34

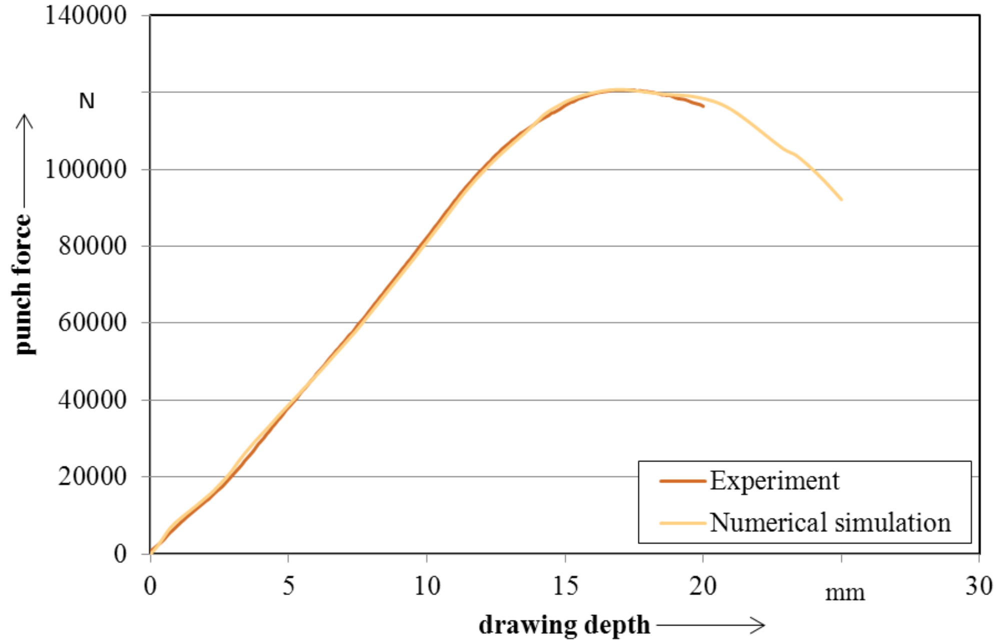

Figure 45 CP-W 800, room temperature, graphite

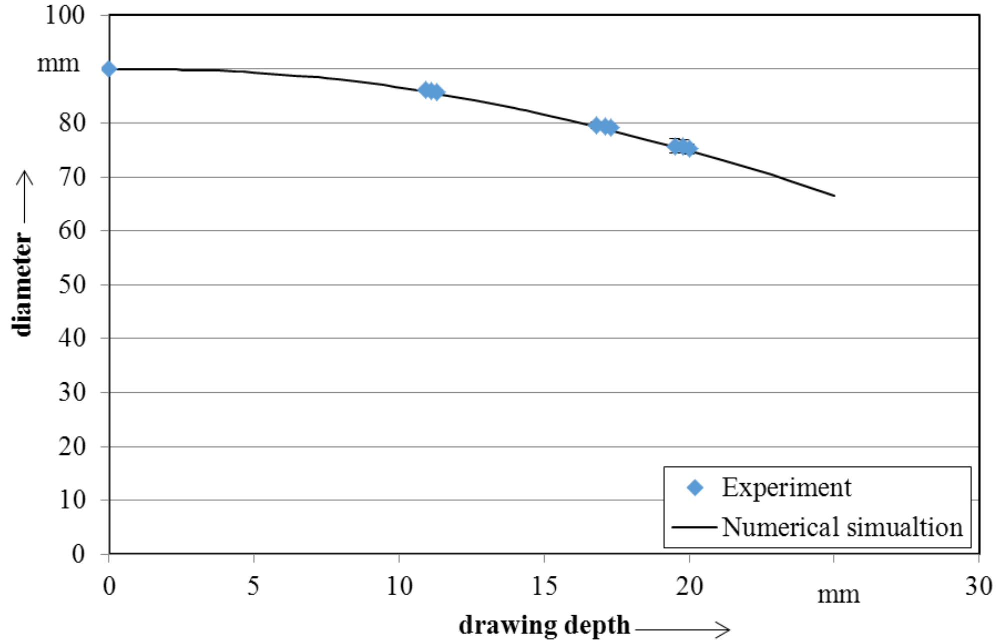

Figure 46 CP-W 800, room temperature, graphite

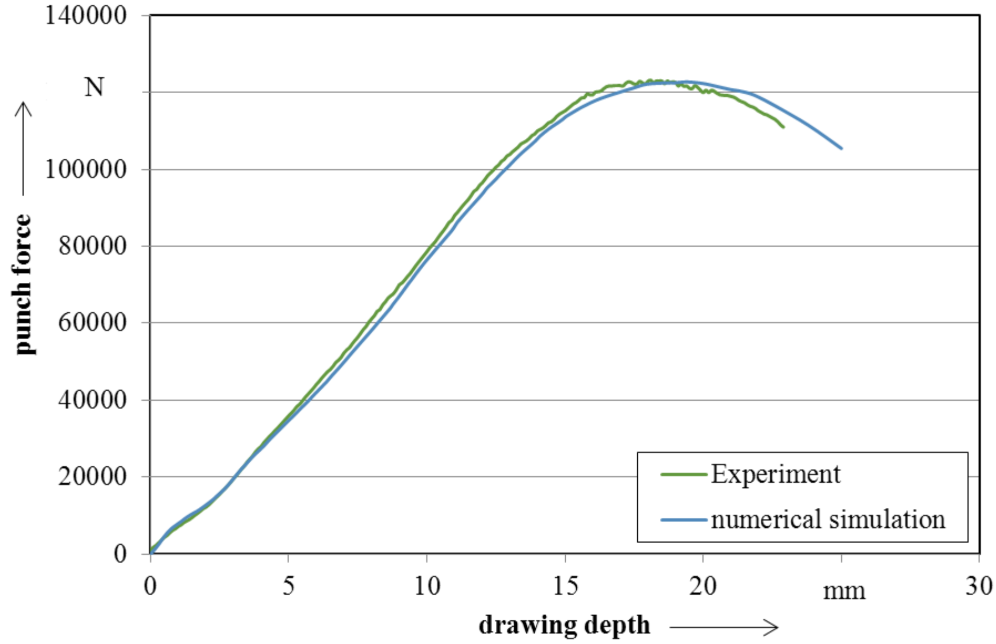

Figure 47 CP-W 800, 500 °C, no lubricant

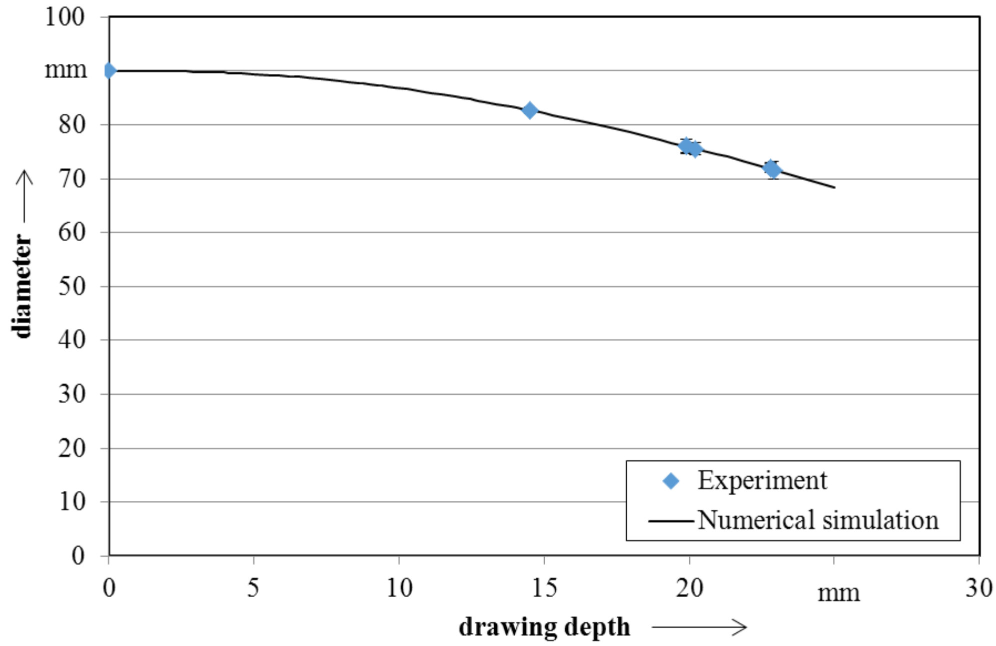

Figure 48 CP-W 800, 500 °C, no lubricant

The evolution of the punch force in the numerical simulation fits the one of the experiments accurately, especially for the case with low friction coefficient. For higher friction coefficient the fit in the initial part is accurate but the punch force in the numerical simulation reach the maximum at a higher drawing depth.

The evolution of the external diameter fits also accurately the measurements conducted in the experimental tests at different drawing depth. This parameter is very important for the calculation of the punch force using the analytical equation of Siebel because the ideal force of deformation in the flange area and especially the contribute of the friction between the blank and the die and between the blank and the blank older are widely influenced by this parameter.

The results of the simulation do not present substantial differences compared with the result of the experiments and the model can be considered accurate and its results precise.

The friction coefficient´s values were calculated matching the result of the maximum punch force evaluated with the experiments and the maximum punch force calculated with the numerical simulation described in the Chapter 5.1. After the evaluation of the friction coefficients it is possible to compere the different lubrication condition also between different temperatures and it is also possible to have quantitative results. It is evident that as the temperature increases, the friction coefficient increases for every lubrication condition. As a consequence of that, it is clear that the major effect in the decrease of punch force is due to the decrease of strength of the material as the temperature increase. The graphite is the most performing lubricant in any condition and in particular as the temperature increases the gap with the other tests increase. The boron nitride gets worse result also compare with the condition without any lubricant and at 600 °C there are no results because all the tests failed.

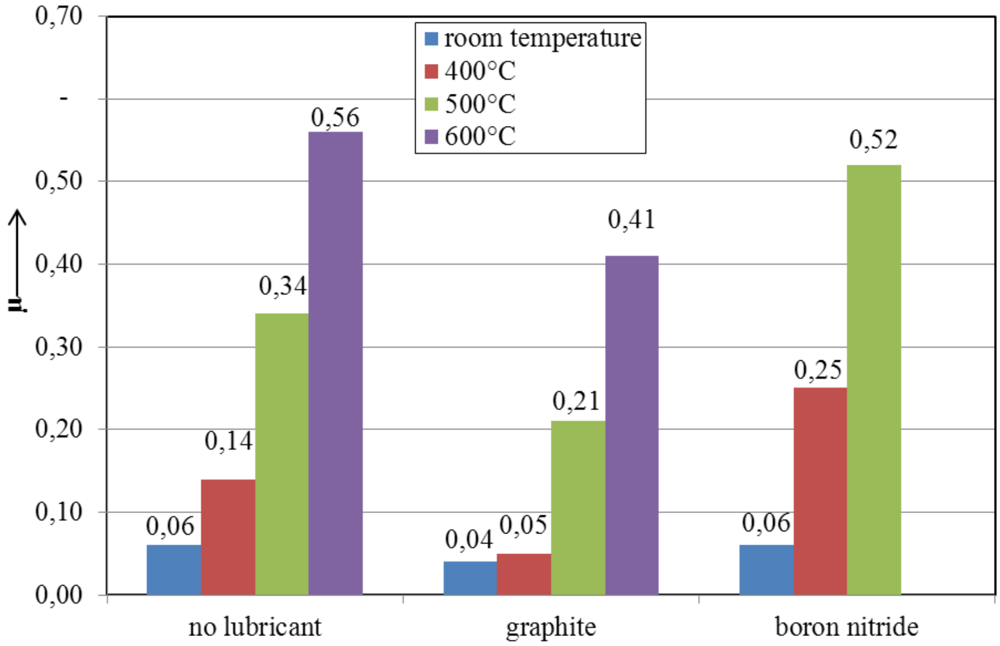

Figure 49 CP-W800 numerical simulation´s friction coefficients sorted by lubricant

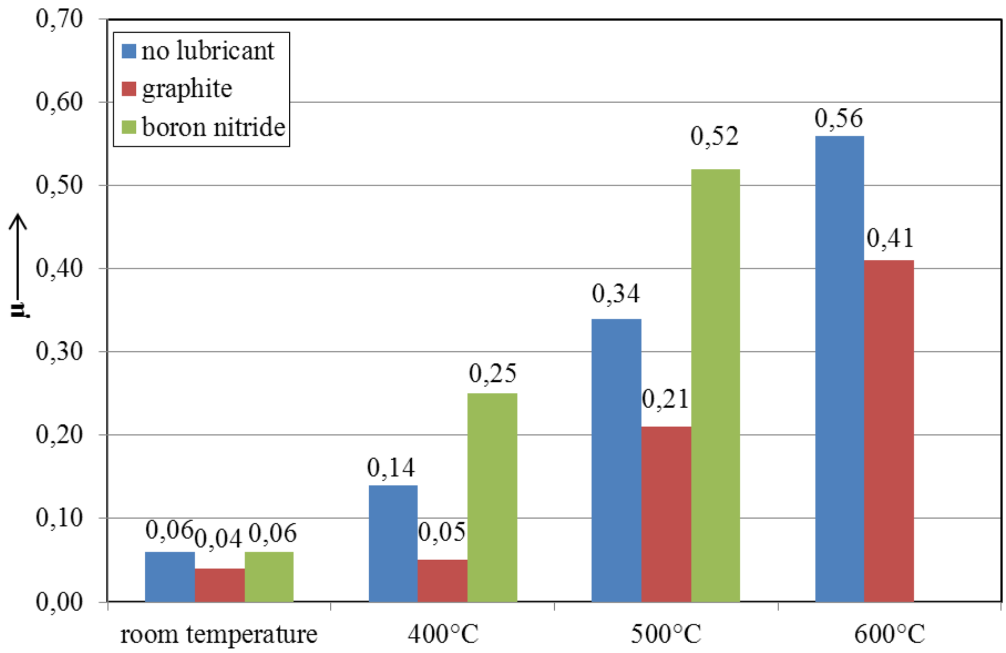

Figure 50 CP-W800 numerical simulation´s friction coefficients sorted by temperature

In the following table all the parameter and result of the analysis are summarized.

Table 12

	Lubricant	**Experiments [N]**	**Simulations [N]**	**μ**
room temperature	-	123900	125015	**0,06**
room temperature	graphite	121767	121799	**0,04**
room temperature	boron nitride	124617	125015	**0,06**
400 °C	-	121486	122409	**0,14**
400 °C	graphite	109914	109887	**0,05**
400 °C	boron nitride	138629	138880	**0,25**
500 °C	-	122500	122573	**0,34**
500 °C	graphite	104140	105585	**0,21**
500 °C	boron nitride	149220	149050	**0,52**
600 °C	-	127840	127331	**0,56**
600 °C	graphite	103117	107565	**0,41**
600 °C	boron nitride	-	-	-

6.1.3 Analytical calculation of friction coefficients

The friction coefficient´s values were also calculated analytically by means of the Siebel formula as described in the Chapter 5.2. This analytical investigation evaluates results that have values lower of about 10% in respect to numerical simulation. The increments on friction coefficient as the temperature increase are in any lubrication condition the same.

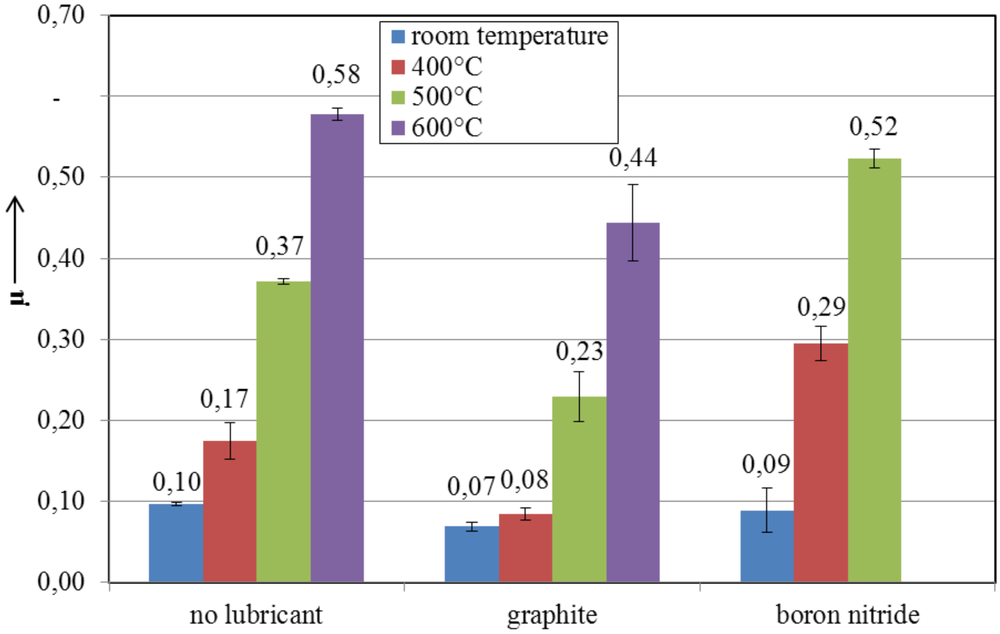

Figure 51 CP-W800 analytical friction coefficients sorted by lubricant

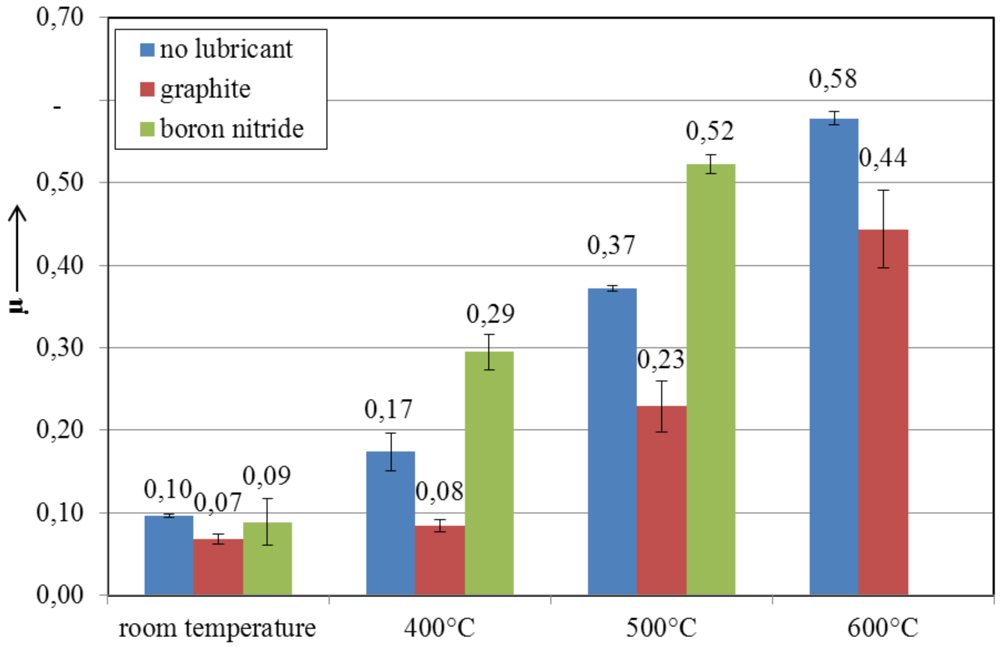

Figure 52 CP-W800 analytical friction coefficients sorted by temperature

In the following table all the parameter and result of the analysis are summarized.

Table 13 CP-W800 friction coefficients summary

	Lubricant	**β**	**ϕ_1**	**ϕ_2**	**ϕ_3**	**K_{fmI}**	**K_{fmII}**	**μ**
room temperature	-	1,6	0,12	0,17	0,29	938	982	0,10
room temperature	graphite	1,6	0,12	0,17	0,29	935	979	0,07
room temperature	boron nitride	1,6	0,14	0,18	0,31	946	988	0,09
400 °C	-	1,6	0,12	0,16	0,29	856	893	0,17
400 °C	graphite	1,6	0,12	0,17	0,29	858	895	0,08
400 °C	boron nitride	1,6	0,15	0,19	0,32	871	904	0,29
500 °C	-	1,6	0,13	0,18	0,30	679	697	0,37
500 °C	graphite	1,6	0,12	0,16	0,29	674	694	0,23
500 °C	boron nitride	1,6	0,13	0,18	0,30	680	698	0,52
600 °C	-	1,6	0,13	0,17	0,30	502	512	0,58
600 °C	graphite	1,6	0,13	0,18	0,30	503	512	0,44
600 °C	boron nitride	-	-	-	-	-	-	

6.1.4 Comparison

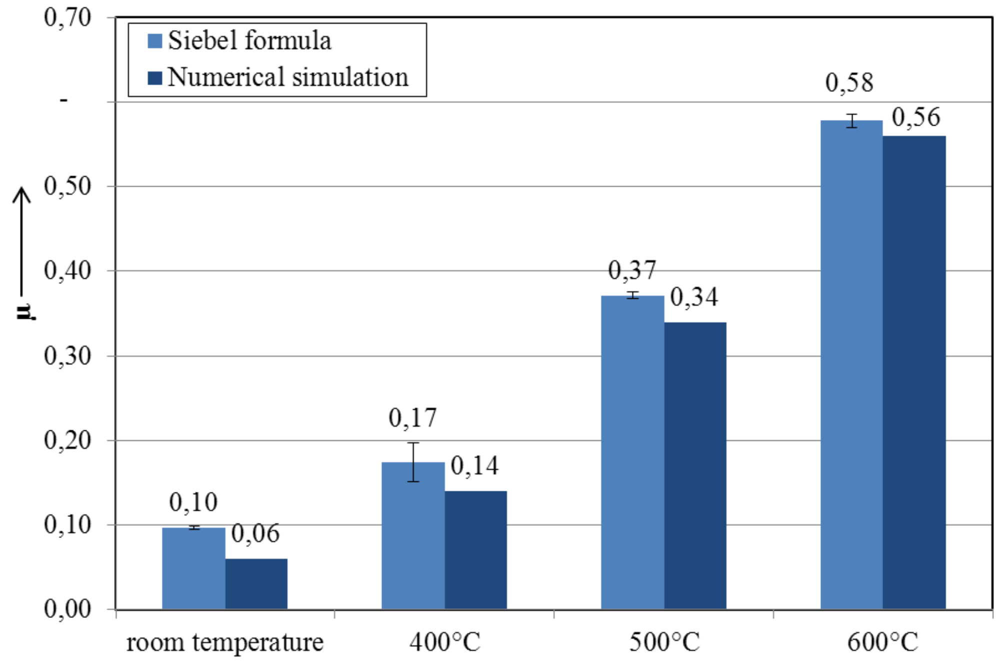

Figure 53 CP-W800, no lubricant

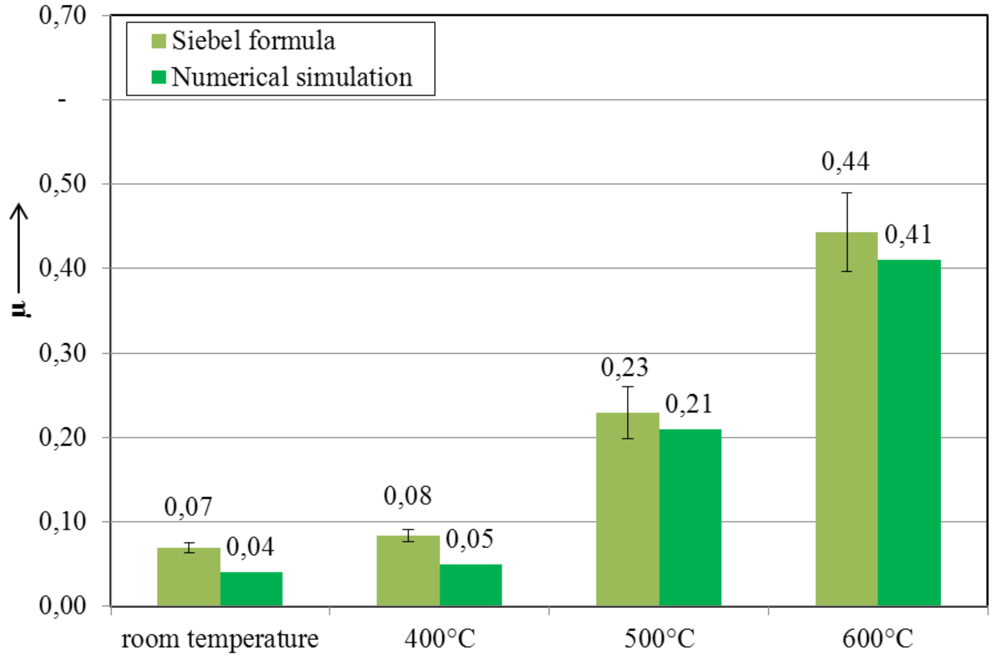

Figure 54 CP-W800, graphite

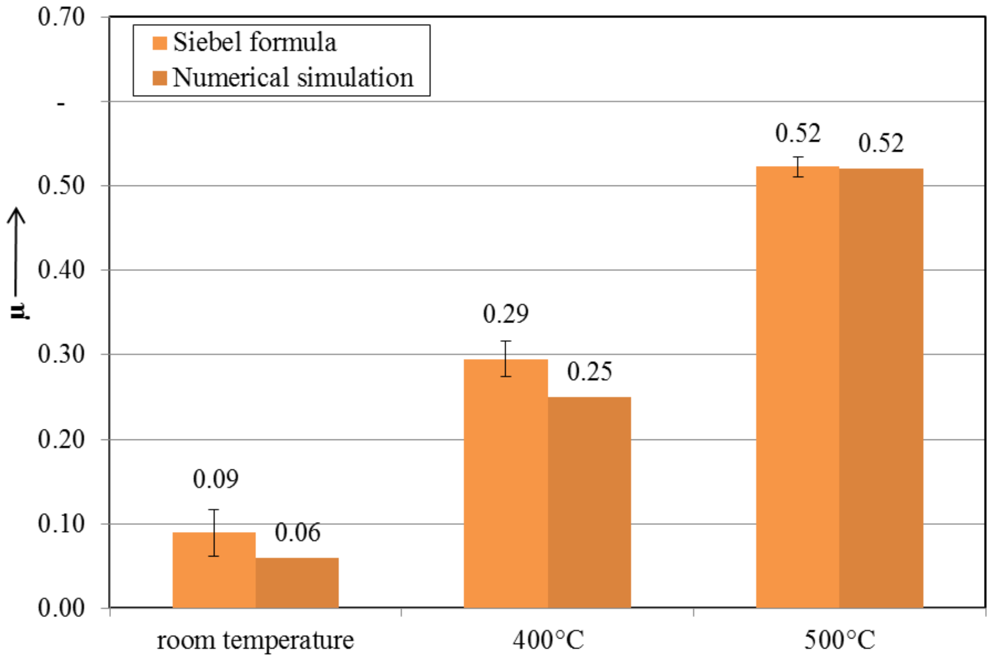

Figure 55 CP-W 800, boron nitride

6.2 MS-W1200

6.2.1 Experiment results

6.2.1.1 Tensile tests

The flow curves, results of the tensile test for the material MS-W1200 are summarized in the following figure. The curves were extrapolated up to a strain rate value of 1. The error bar represents the standard deviation calculated between the values of the four replications conducted for every temperature.

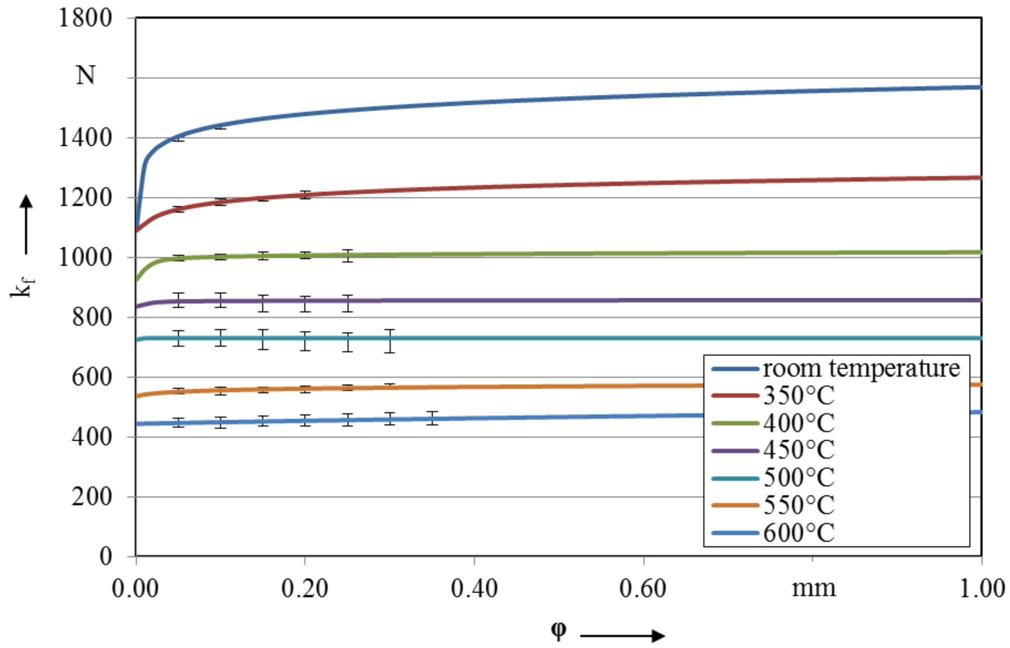

Figure 56 MS-W1200 flow curves

As the temperature increase, the strength needed for the deformation of the material decrease and also the elongation reach higher values.

For this material the Swift-Voce interpolation formula was used:

$$k_f = a \cdot k_{f\,swift}(\varphi) + (1 - a) \cdot k_{f\,voce}(\varphi) \qquad [\,64\,]$$

This formula combines the result of the interpolation of the Swift formula

$$k_f = b \cdot (a + \varphi)^c \qquad [\,65\,]$$

and the result of the Voce formula

$$k_f = b - (b - a)exp^{-c \cdot \varphi} \qquad [\,66\,]$$

The calculated coefficients are summarized in the following table.

Table 14 MS-W1200 Swift coefficients

Swift	**a**	**b**	**c**	**d**	**e**	**f**
room temperature	0,000	1570	0,037	-	-	-
350 °C	0,002	1267	0,029	-	-	-
400 °C	0,000	1019	0,008	-	-	-
450 °C	0,000	859	0,003	-	-	-
500 °C	0,141	730	0,000	-	-	-
550 °C	0,009	575	0,015	-	-	-
600 °C	0,942	447	0,116	-	-	-

Table 15 MS-W1200 Voce coefficients

Swift	**a**	**b**	**c**	**d**	**e**	**f**
room temperature	0,001	1523	52	-	-	-
350 °C	0,007	1249	10	-	-	-
400 °C	0,007	1012	63	-	-	-
450 °C	0,008	856	139	-	-	-
500 °C	0,014	730	814	-	-	-
550 °C	0,006	570	21	-	-	-
600 °C	0,019	512	1	-	-	-

Table 16 MS-W1200 Swift-Voce coefficients

Swift	a	b	c	d	e	f
room temperature	0,98	-	-	-	-	-
350 °C	0,99	-	-	-	-	-
400 °C	0,76	-	-	-	-	-
450 °C	0,48	-	-	-	-	-
500 °C	0,00	-	-	-	-	-
550 °C	1,02	-	-	-	-	-
600 °C	1,07	-	-	-	-	-

6.2.1.1.1 Influence of strain rate

The flow curve change due to the higher strain rate is not the same for all the temperature. In any conditions there are differences in the flow curves, especially for higher temperature.

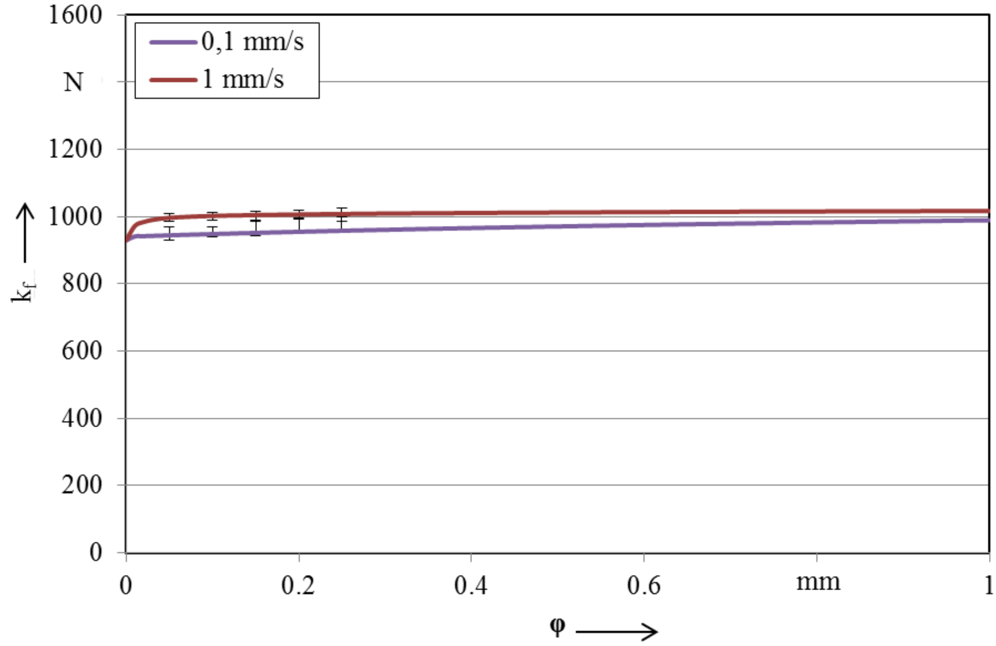

Figure 57 MS-W1200 influence of the strain rate on the flow curves at 400 °C

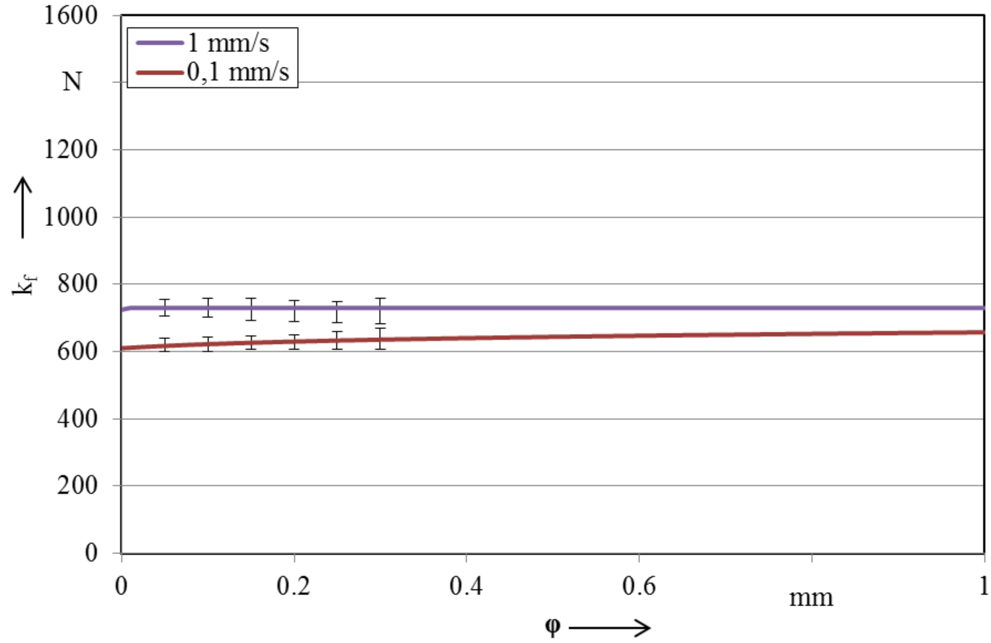

Figure 58 MS-W1200 influence of the strain rate on the flow curves at 500 °C

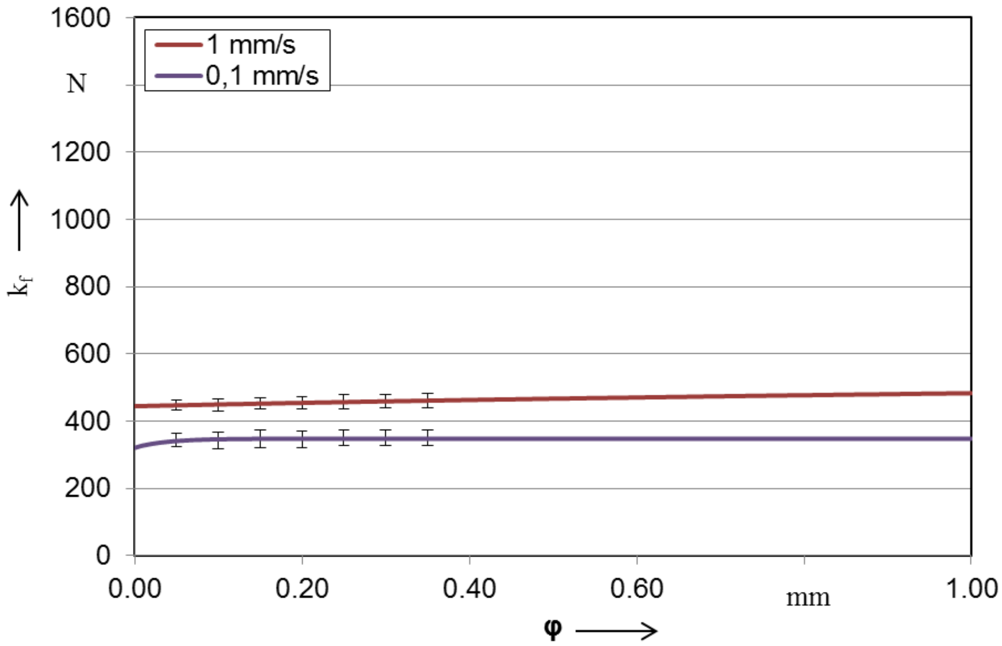

Figure 59 MS-W1200 influence of the strain rate on the flow curves at 600 °C

6.2.1.2 Cup deep drawing tests

The MS-W1200 shows a different behavior of the lubricant conditions compared to the CP-W800. The influence of the temperature on the material strength is very noticeable, the maximum punch force decrease with the temperature in any lubricant condition, and so it is not possible to say if the friction coefficient increase or stay constant with the temperature. At room temperature the different lubricant conditions does not have big influence in the punch force but as the temperature increase the graphite is the most performing lubricant. The boron nitride gets worse results compare also to the condition without any lubricant and at 600°C there are no result because every test failed.

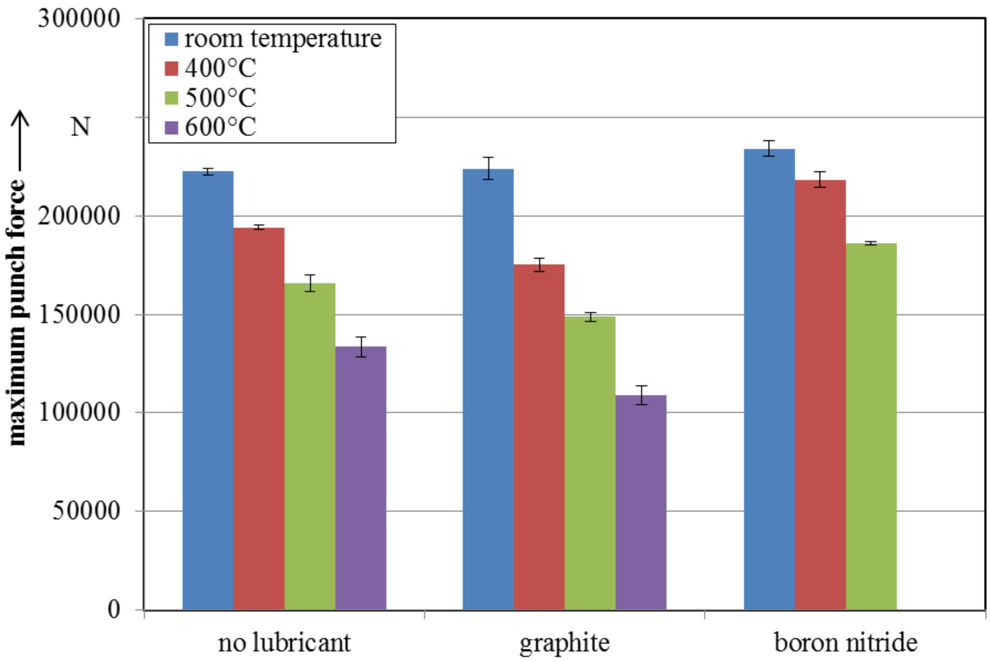

Figure 60 MS-W1200 Maximum punch force sorted by lubricant

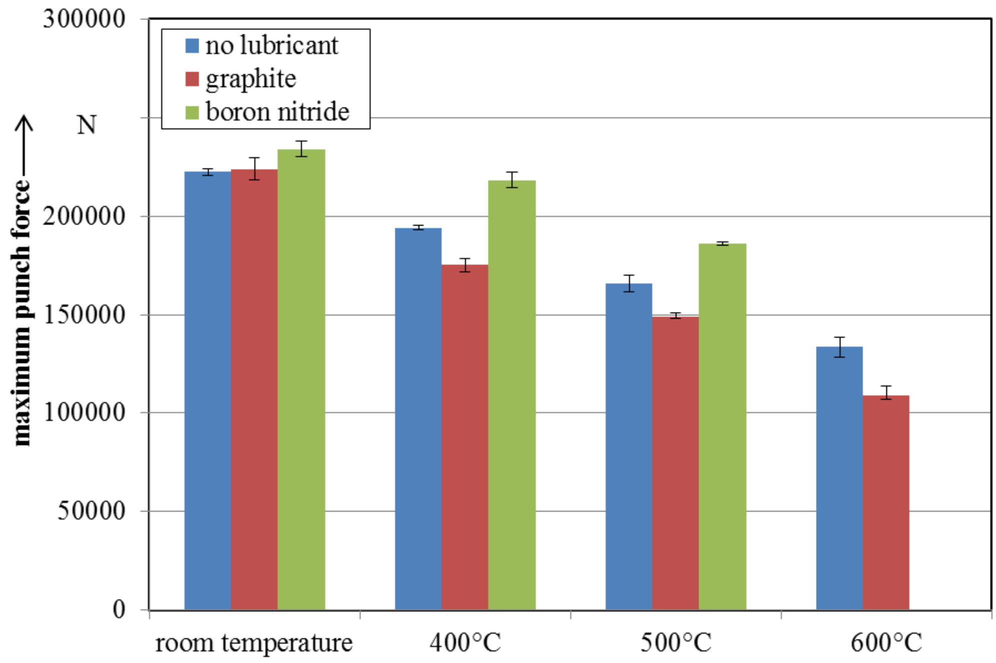

Figure 61 MS-W1200 Maximum punch force sorted by temperature

In the table the test conditions and the test outputs are summarized, the maximum force is calculated as an average of the three tests with drawing depth above the maximum force and also the standard deviation is calculated from the same data. The maximum force diameter is calculated with the formula obtained by the interpolation of the flange diameters of the specimens as a function of the drawing depth.

Table 17 MS-W1200 cup deep drawing test summary

	Lubricant	**max force [N]**	**D [mm]**	**BHF [N]**	**velocity [mm/s]**
room temperature	-	222267	80,15	31702	27
room temperature	graphite	223833	80,18	26430	26
room temperature	boron nitride	233883	80,17	31429	27
400 °C	-	194133	80,44	18675	22
400 °C	graphite	175133	79,90	17834	16
400 °C	boron nitride	218217	80,42	18083	18
500 °C	-	165667	79,19	18046	17
500 °C	graphite	148767	79,09	17988	17
500 °C	boron nitride	185933	79,70	17971	18
600 °C	-	133467	80,01	17066	19
600 °C	graphite	108960	78,74	16971	19
600 °C	boron nitride				

6.2.2 Numerical calculation of friction coefficients

In this investigation the interested output is the punch force, so the reaction force in vertical direction of the punch is exported. As a consequence of the representation of the punch as analytical rigid body it cannot be meshed and so the reaction force is not computed in a node but in correspond to the reference point.

It is plotted the punch force-drawing depth graphic and the external diameter-drawing depth graphic calculated by means of the numerical simulation, in order to create this graphic the displacement of the punch and of the node in the midpoint of the thickness in the external diameter of the blank is exported. This graphics can be plotted together with the experimental data and confront with them. It is done this qualitative comparison between a condition with low friction coefficient and a condition and with a high friction coefficient:

- MS-W1200
- Graphite
- Room temperature
- Friction coefficient 0,04

And

- MS-W1200
- No lubricant
- 500°C
- Friction coefficient 0,4

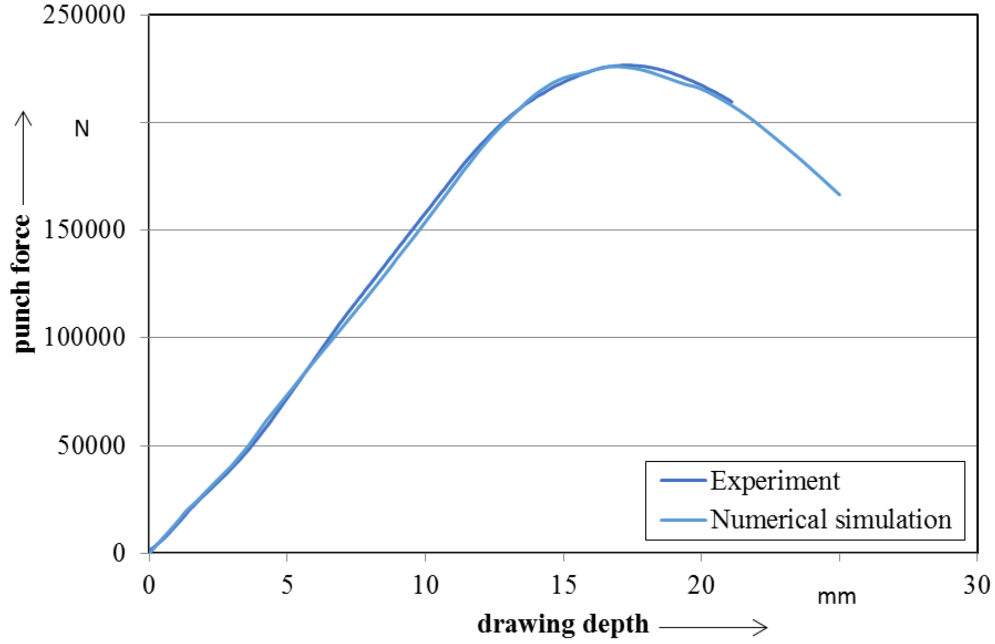

Figure 62 MS-W1200, room temperature, graphite

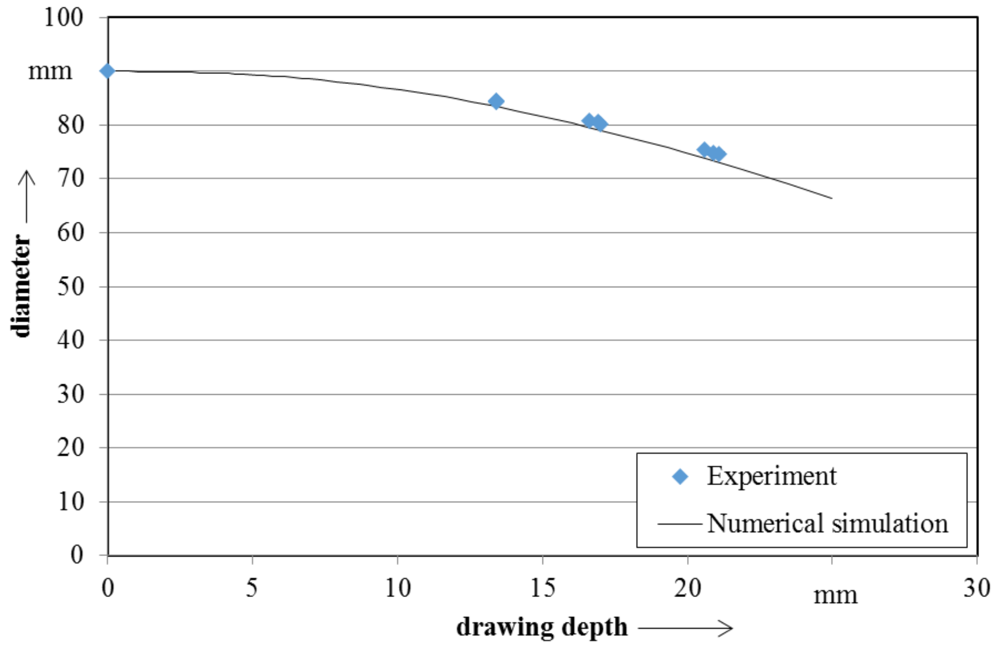

Figure 63 MS-W1200, room temperature, graphite

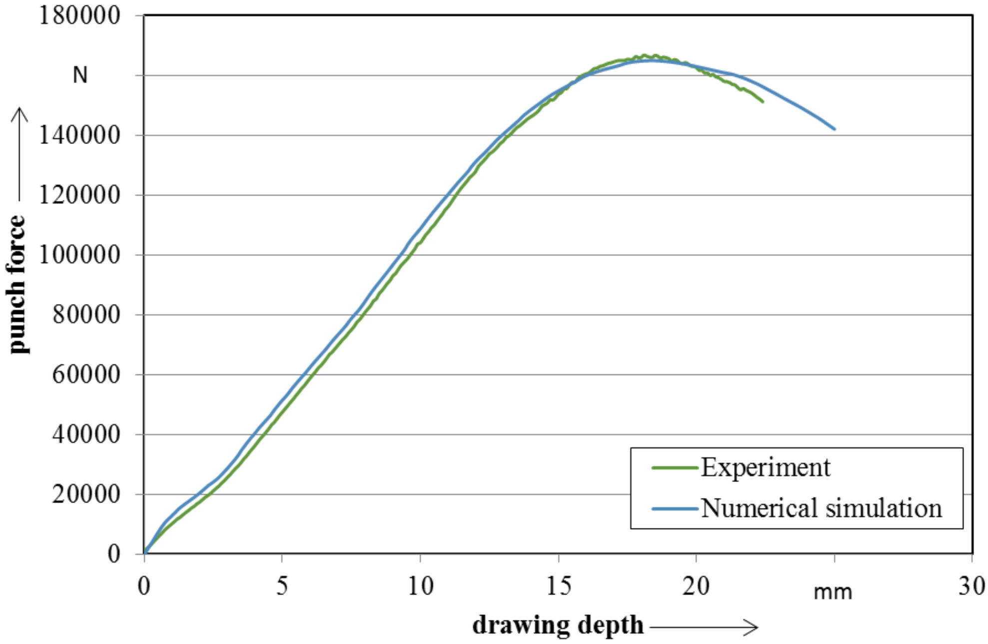

Figure 64 MS-W1200, 500°C, no lubricant

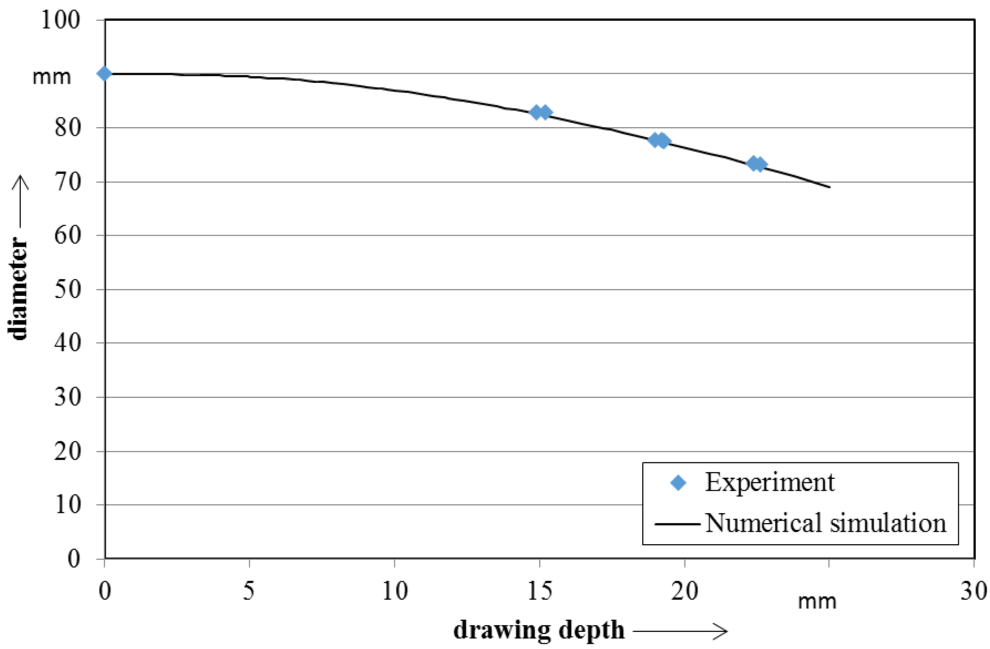

Figure 65 MS-W1200, 500°C, no lubricant

The evolution of the punch force in the numerical simulation fits the one of the experiments accurately.

The evolution of the external diameter fits also accurately the measurements conducted in the experimental tests at different drawing depth. This parameter is very important for the calculation of the punch force using the analytical equation of Siebel because the ideal force of deformation in the flange area and especially the contribute of the friction between the blank and the die and between the blank and the blank older are widely influenced by this parameter.

The results of the simulation do not present substantial differences compared with the result of the experiments and the model can be considered accurate and its results precise.

The friction coefficient´s value were calculated matching the result of the maximum punch force evaluated with the experiments and the maximum punch force calculated with the numerical simulation described in the Chapter 5.1. The MS-W1200 shows a different behavior of the punch force compare with the CP-W800 but the behavior of the friction coefficient doesn´t show big differences. At room temperature the friction coefficient are similar and as the temperature increase the friction coefficient drops for any friction condition (the punch force shows a decreasing trend in any case). Graphite shows the best performance for every temperature and its evolution with the temperature tends to the linearity. For the other lubricant conditions the friction coefficient´s value increase quickly for low temperature and slower at higher temperature. The boron nitride gets worse result and for 600°C there are not results because all the tests failed.

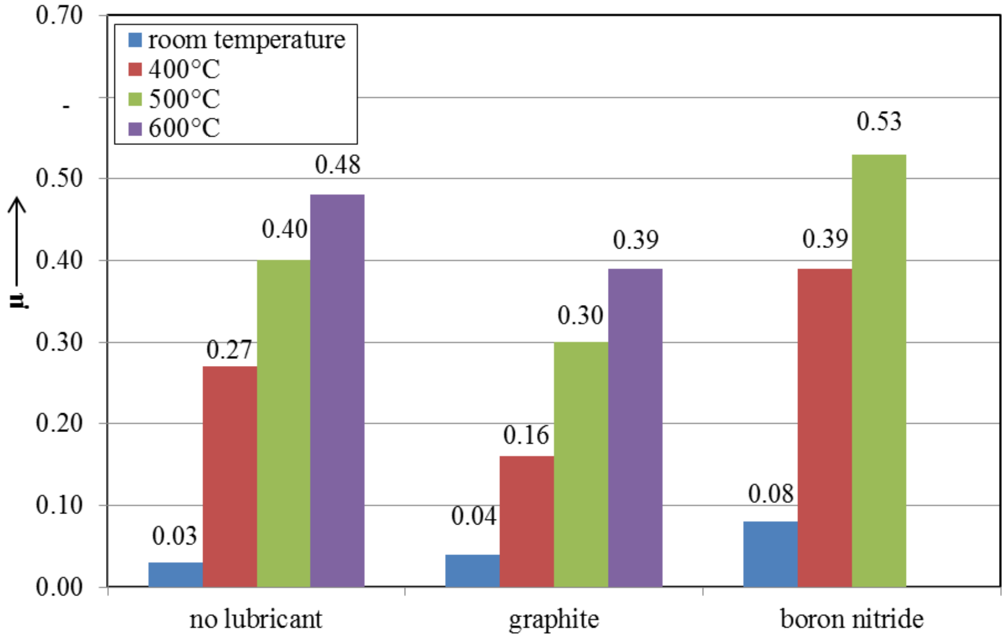

Figure 66 MS-W1200 numerical simulation´s friction coefficients sorted by lubricant

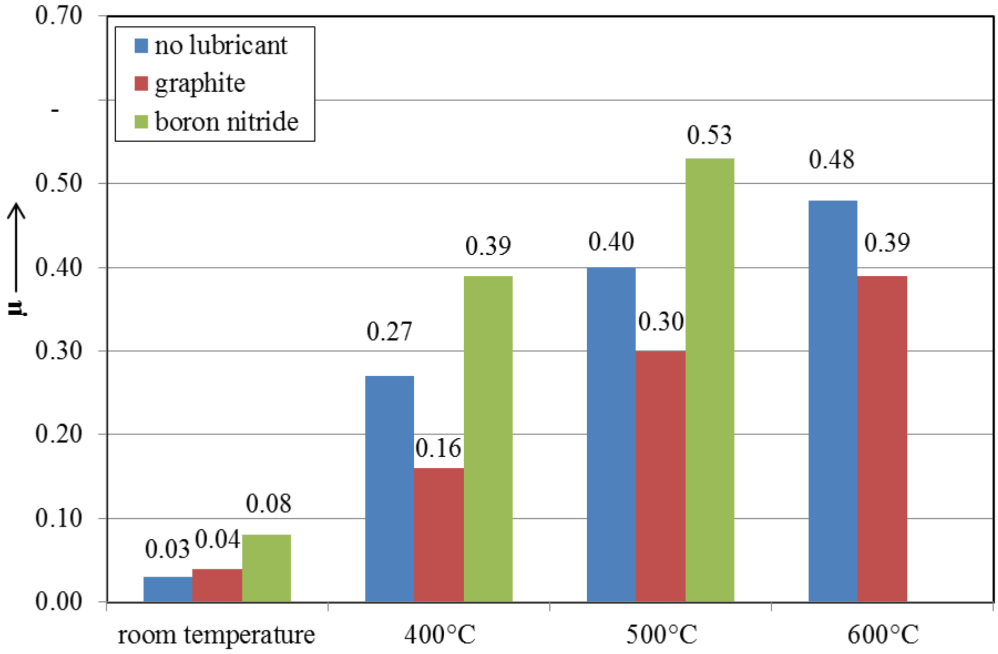

Figure 67 MS-W1200 numerical simulation´s friction coefficients sorted by temperature

In the following table, all the parameter and result of the analysis are summarized.

Table 18

	Lubricant	**Experiments [N]**	**Simulations [N]**	**µ**
room temperature	-	222267	222783	**0,03**
room temperature	graphite	223833	224464	**0,04**
room temperature	boron nitride	233883	233318	**0,08**
400 °C	-	194133	193818	**0,27**
400 °C	graphite	175133	175159	**0,16**
400 °C	boron nitride	218217	218542	**0,39**
500 °C	-	165667	164522	**0,4**
500 °C	graphite	148767	148975	**0,3**
500 °C	boron nitride	185933	186007	**0,53**
600 °C	-	133467	133700	**0,48**
600 °C	graphite	108960	108307	**0,39**
600 °C	boron nitride	-	-	-

6.2.3 Analytical calculation of friction coefficients

The friction coefficient´s values were also calculated analytically by means of the Siebel formula as described in the Chapter 5.2. The results of the analytical approach for this material fit accurately the values calculated with the numerical approach. Only the results of the evaluation of the friction coefficient for the boron nitrite at 500 °C and 600 °C show an underestimation in respect of the numerical simulation of about 13% on the average.

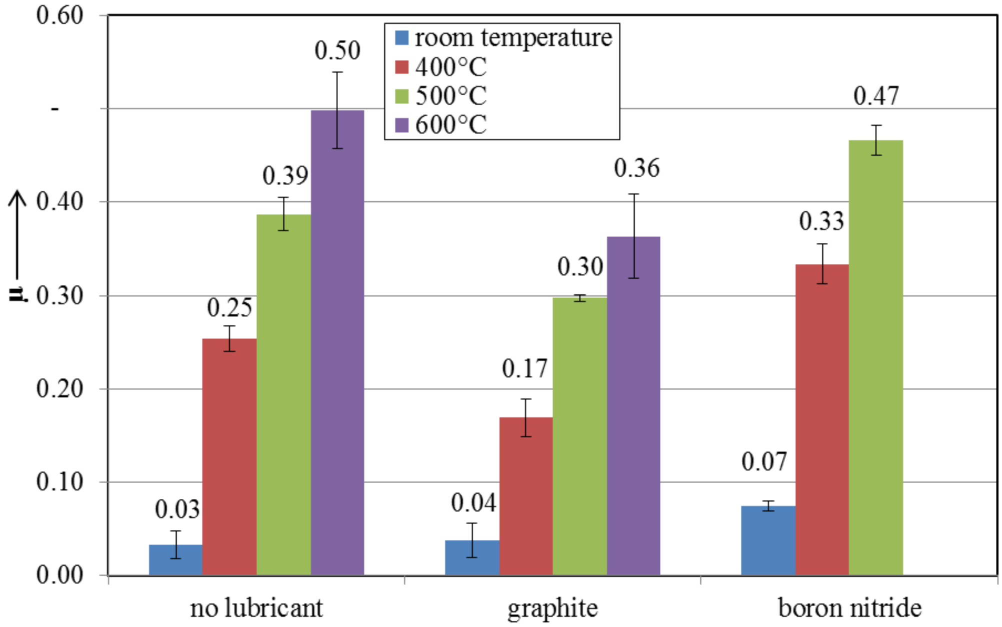

Figure 68

MS-W1200 Friction coefficients sorted by lubricant

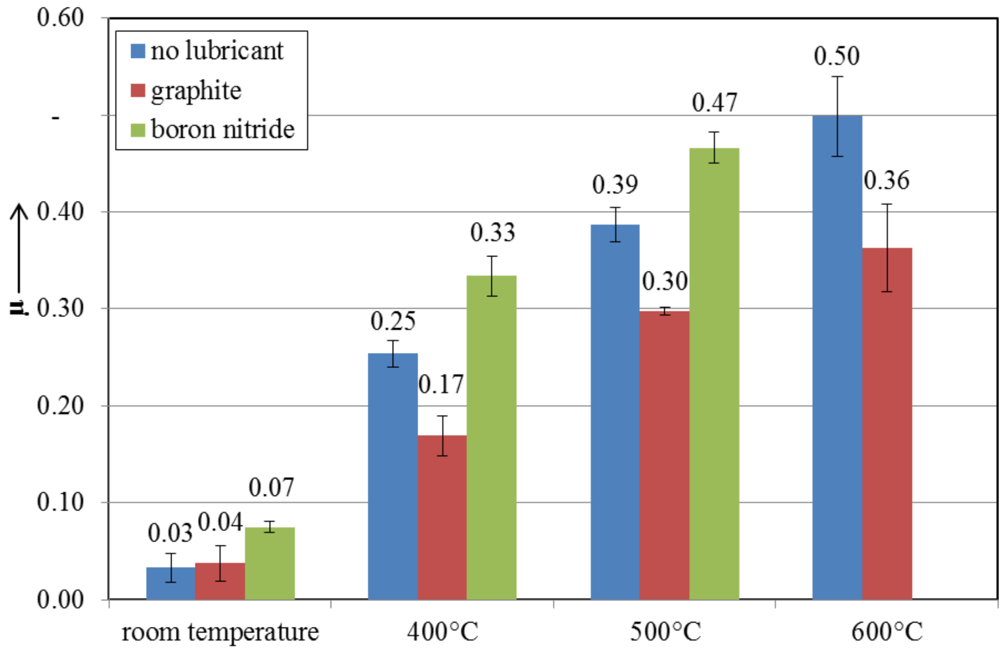

Figure 69 MS-W1200 Friction coefficients sorted by temperature

In the following table all the parameter and result of the analysis are summarized.

Table 19 MS-W1200 friction coefficients summary

	Lubricant	β	ϕ_1	ϕ_2	ϕ_3	K_{fmI}	K_{fmII}	µ
room temperature	-	1,6	0,12	0,16	0,30	1459	1485	0,03
room temperature	graphite	1,6	0,12	0,16	0,30	1459	1485	0,04
room temperature	boron nitride	1,6	0,12	0,16	0,30	1459	1485	0,07
400°C	-	1,6	0,11	0,16	0,30	855	855	0,25
400°C	graphite	1,6	0,12	0,17	0,31	855	855	0,17
400°C	boron nitride	1,6	0,11	0,16	0,30	855	855	0,33
500°C	-	1,6	0,13	0,18	0,32	730	730	0,39
500°C	graphite	1,6	0,13	0,18	0,32	730	730	0,30
500°C	boron nitride	1,6	0,12	0,17	0,31	730	730	0,47
600°C	-	1,6	0,12	0,16	0,31	480	483	0,50
600°C	graphite	1,6	0,13	0,18	0,32	481	483	0,36
600°C	boron nitride	-	-	-	-	-	-	

6.2.4 Comparison

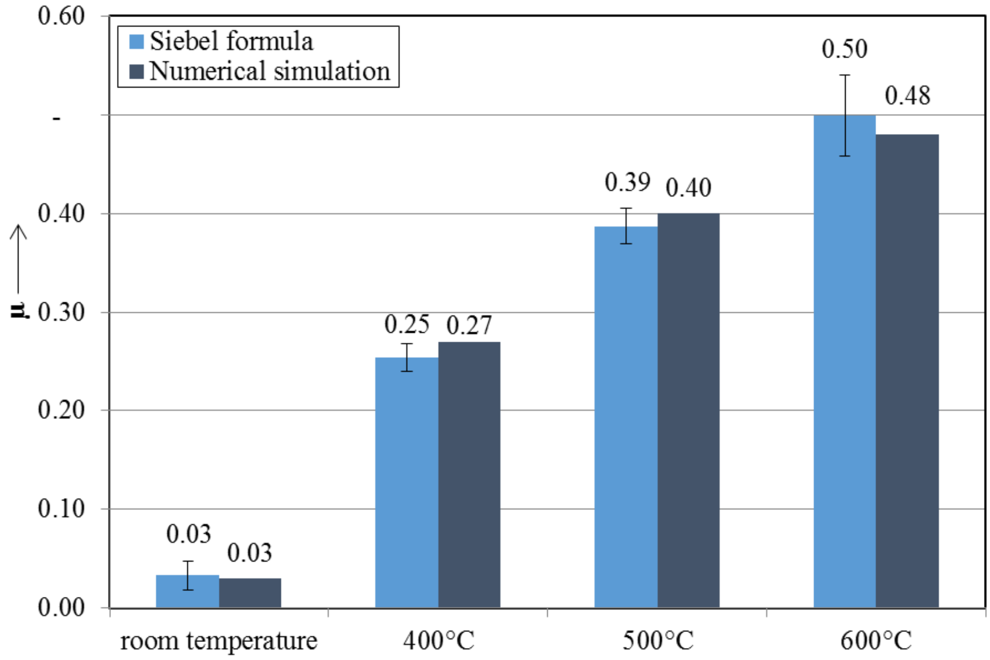

Figure 70 MS-W 1200, no lubricant

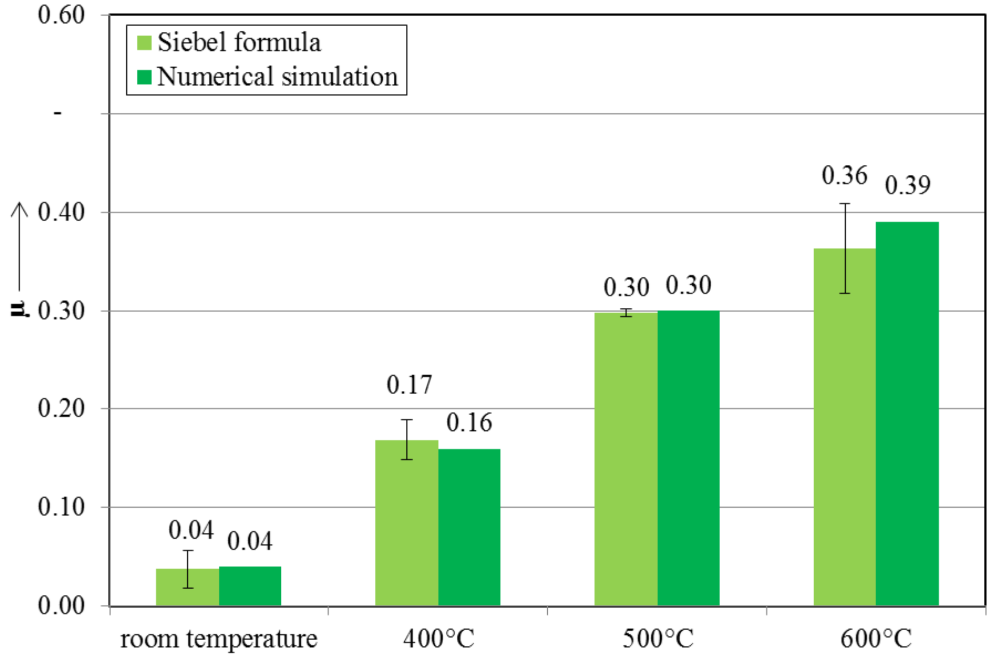

Figure 71 MS-W 1200, graphite

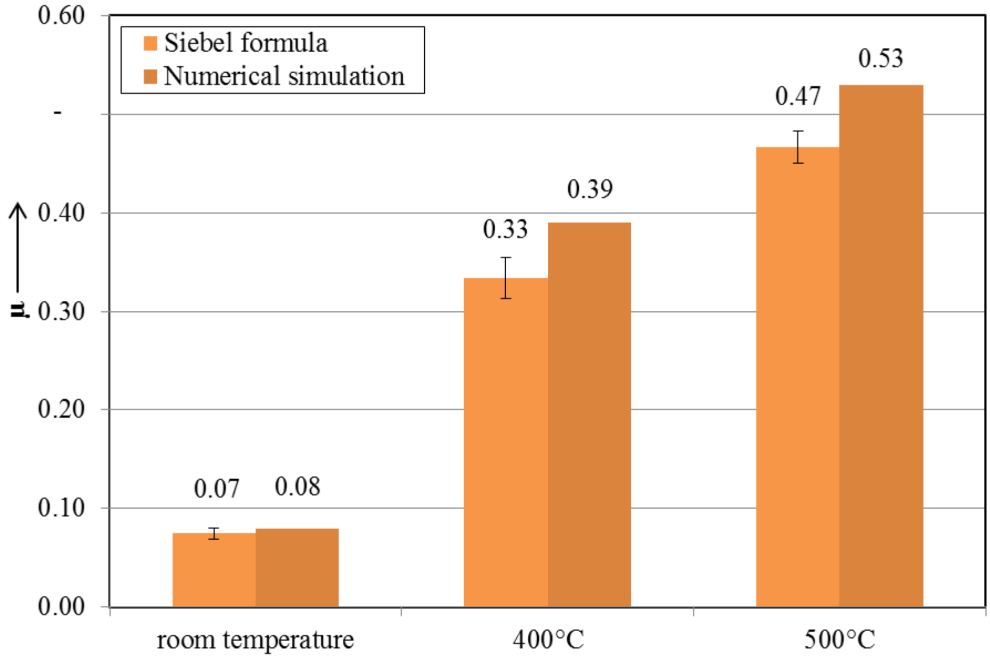

Figure 72 MS-W 1200, boron nitride

7 Summary

Due to the increased importance of the warm forming operation in the manufacturing of high strength steels, the lubricants have gain a very important role in the reduction of friction. The friction coefficient indeed can reach high values for the elevated temperatures. This work presents the characterization of different dry lubricants at different temperatures in deep drawing operations.

In order to investigate the friction behavior, cup deep drawing tests of complex phase steel CP-W800 and the martensitic phase steel MS-W1200 have been carried out. These tests were conducted with practical stamping operation at room temperature, 400 °C, 500 °C and 600 °C.

The specimens were coated with two different dry lubricants, graphite and boron nitride. Tests without lubricant were also carried out in order to confront the contribution in reduction of friction of the lubricants.

During the deep drawing tests, the punch force, measured by means of a load cell, reaches a maximum at a drawing depth that is independent of the lubricant and of the materials. So it was possible to compare the value of the forces for the different conditions in order to get a comparison between the lubricants.

In order to evaluate the friction effect in the punch force, two different approaches have been used: a numerical approach and an analytical approach. In the first approach a 2D axisymmetric numerical simulation by means of ABAQUS software has been conducted. It has been so possible to evaluate the maximum punch force of the process and evaluate the friction coefficient matching the results of the simulation with the experiments.

The analytical approach calculates the maximum punch force by means of the theoretical equation of Siebel based on plasticity theory. The calculation was made taking into account

- the components of ideal force of deformation,
- bending and back bending force,
- friction force between the blank holder and the die,
- friction effect at the radius of the die are.

In order to calculate the component of deformation and bending the flow curves of the materials are need. With this goal, tensile tests at room temperature and elevated temperature were conducted with a “Gleeble” testing machine.

The specimens were heated by Joule effect and the real strain were measured by means of the “Aramis” computer’s vision software.

8 Conclusions

The cup deep drawing tests have been able to evaluate the performance of different stamping lubricants at different temperature.

As the temperature increases, the friction coefficients increase in any lubricant conditions. At room temperature, the lubricants show the same behavior and there are no differences in the forces measured by the load cell of the punch. Consequently, also the friction coefficient does not change with the lubricant at room temperature. As the temperature increases, the evolution of the maximum punch force is different between the materials: the measured forces of the CP-W800 without lubricants maintain the same values for every temperature because as the temperature rises the increment of friction is counterbalanced by the drop of strength of the materials. With the boron nitride, the increment of friction is higher and the forces increase with temperature. On the contrary, the graphite shows a better behavior of the friction and the forces drops as the temperature increase.

The MS-W1200 is more influenced in the strength by the temperature insomuch that the reduction of strength from 400 °C and 600 °C is about 70% in the ultimate tensile stress. Consequently for every lubricants the maximum punch force decrease with the temperature but also in this case the graphite shows the best performance.

For both materials, the boron nitride gets worse result also compared with the no lubricant conditions and at 600 °C it was no possible to have results because all the tests failed as a consequence of the increase of friction.

In order to evaluate quantitatively the friction coefficient, the process was numerically simulated with the software “Abaqus”. The results of the numerical simulations, computed with a 2D axisymmetric model, show good agreement with the experimental data. The calculated curves, indeed, fits precisely the experiments and the maximum punch force is reached at the same drawing depth.

Once the numerical simulation has been computed, it was not only possible to evaluate the friction coefficient but also to compare the friction contribution between the different temperatures. This comparison was not possible with the punch force because it is influenced by the strength of the material that changes with the temperature.

The friction coefficient of the CP-W800 lubricated with graphite is almost the same for room temperature and 400 °C; for higher temperature it increase linearly. Without lubricant, the behavior is similar but all the increments due to temperature are higher.

The friction coefficient of the MS-W1200 lubricated with graphite show a linear behavior with the temperature up to 500 °C; at 600 °C, the increment is lower than the linearity. In the other lubricant conditions the friction coefficient is subjected to an elevated increment from room temperature up to 400 °C and then it progress linearly.

For both materials, the graphite shows the best lubrication properties in terms of reduction of friction and the boron nitride gets worse result increasing the friction contribution also compared to the no lubricant condition.

In order to have a compare and a confirmation about the goodness of the results, the friction coefficients were also calculated analytically by means of the theoretical equation of Siebel based on plasticity theory.

The results of this approach show a good agreement with the results of the numerical simulation and the behavior of the materials in the different lubricant conditions is almost the same. The friction coefficient calculated for the CP-W800 has values lower of about 10% in respect to numerical simulation.

The friction coefficient calculated for the MS-W1200 has the same values of the numerical simulation considering the standard deviation calculated from the repetitions of the experiments. Only the results of the friction coefficient for the boron nitrite at 500°C and 600°C show an underestimation in respect of the numerical simulation of about 13% on the average.

As a consequence of the accordance between the results of numerical and analytical approach, it is possible to conclude that the friction coefficients calculated in this investigation can be considered valid.

9 Bibliography

A. Ghiotti, S. B. (2010). Tribological characteristics of high strength steel sheets under hot stamping conditions. *Journal of Materials Processing Technology*.

Abaqus. (n.d.). *Abaqus manual.* Retrieved from www.lft.uni-erlangen.de/v6.11/

Andreini, P. (2002). *Manuale dell´ ingegnere meccanico.* Milano: Hoepli.

Boljanovic, V. (2004). *Sheet metal forming process and die design.* New York: Industrial press inc.

Chandrasekharan, S., & Hariharasudhan Palaniswamy, N. J. (2005). Evaluation of stamping lubricants at various temperature levels using the ironing test. *International Journal of Machine Tools and Manufacture*, 379–388.

Eckart Doege, B.-A. B. (2010). *Handbuch Umformtechnik: Grundlagen, Technologien, Maschinen.* Hannover: Springer.

ESK. (n.d.). Retrieved from Ekamold EP aerosol boron nitride spray.

Feinblech, S. V.-U. (2006, July). Testing and Documentation Guideline for the Experimental Determination of Mechanical Properties of Steel Sheets for CAE-Calculations. Düsselndorf.

H. Karbasian, A. T. (2010). A review on hot stamping. *Journal of Materials Processing Technology*, 2103–2118.

Hyunok Kim, J. H. (2007). Evaluation of stamping lubricants using the deep drawing test. *International Journal of Machine Tools and Manufacture*, 2120–2132.

Hyunok Kim, T. A. (2009). Evaluation of stamping lubricants in forming advanced high strength steels (AHSS) using deep drawing and ironing tests. *Journal of Materials Processing Technology*, 4122–4133.

kemie, K. (n.d.). Retrieved from Graphit 33 technical data sheet.

Lange, K. (1975). *Handbook of Metal Forming.* Stuttgart: McGraw-Hill Book Company.

Lange, K. (1988). *Handbuch für Industrie und Wissenschaft.* Berlin Heidelberg New York London Paris Tokio: Springer-Verlag.

N.Ethirai, V. K. (2012). Finite Element Method Based Simulation on Warm Deep Drawing of AISI 304 Steel Circular Cups. *International Conference on Modeling Optimisation and Computing.*

Nisture, S. P. (2006). *Engineering Mechanics.* Pune: Technical Publications Pune.

R. Neugebauer, T. A. (2006). Sheet metal forming at elevated temperatures. *CIRP Annals - Manufacturing Technology*, 793–816.

Serope Kalpakjian, S. R. (2008). *Tecnologia meccanica.* Pearson Paravia Bruno mondadori s.p.a.

Stahl, T. (n.d.). *Forming properties of high-strength and ultrahigh-strength multi-phase steels.*

Strffellini, G. (2005). *Attrito e usura. Metodologie di progettazione e controllo.* Trento: Tecniche nuove.

Z.Hu, H. S. (2003). Determination of Friction Coefficient in Deep Drawing. *1st Colloquium Processscaling.* Bremen.

10 Acknowledgements